ARTICLE

doi:10.1038/nature21029

Neurotoxic reactive astrocytes are induced by activated microglia

Shane A. Liddelow[1,2], Kevin A. Guttenplan[1], Laura E. Clarke[1], Frederick C. Bennett[1,3], Christopher J. Bohlen[2], Lucas Schirmer[4,5], Mariko L. Bennett[1], Alexandra E. Münch[1], Won-Suk Chung[6], Todd C. Peterson[7], Daniel K. Wilton[8], Arnaud Frouin[8], Brooke A. Napier[9], Nikhil Panicker[10,11,12], Manoj Kumar[10,11,12], Marion S. Buckwalter[7], David H. Rowitch[13,14], Valina L. Dawson[10,11,12,15,16], Ted M. Dawson[10,11,12,16,17], Beth Stevens[8] & Ben A. Barres[1]

Reactive astrocytes are strongly induced by central nervous system (CNS) injury and disease, but their role is poorly understood. Here we show that a subtype of reactive astrocytes, which we termed A1, is induced by classically activated neuroinflammatory microglia. We show that activated microglia induce A1 astrocytes by secreting Il-1α, TNF and C1q, and that these cytokines together are necessary and sufficient to induce A1 astrocytes. A1 astrocytes lose the ability to promote neuronal survival, outgrowth, synaptogenesis and phagocytosis, and induce the death of neurons and oligodendrocytes. Death of axotomized CNS neurons *in vivo* is prevented when the formation of A1 astrocytes is blocked. Finally, we show that A1 astrocytes are abundant in various human neurodegenerative diseases including Alzheimer's, Huntington's and Parkinson's disease, amyotrophic lateral sclerosis and multiple sclerosis. Taken together these findings help to explain why CNS neurons die after axotomy, strongly suggest that A1 astrocytes contribute to the death of neurons and oligodendrocytes in neurodegenerative disorders, and provide opportunities for the development of new treatments for these diseases.

Astrocytes are abundant cells in the CNS that provide trophic support for neurons, promote formation and function of synapses, prune synapses by phagocytosis, and fulfil a range of other homeostatic maintenance functions[1–4]. Astrocytes undergo a pronounced transformation called 'reactive astrocytosis' after brain injury and disease, whereby they upregulate many genes[5,6] and form a glial scar after acute CNS trauma[1,6,7]. Functions of reactive astrocytes have been a subject of some debate, with previous studies showing that they can both hinder and support CNS recovery[1,6–9]. It has not been clear in which context these cells may be helpful or harmful and many questions remain about their functions.

We previously purified and genetically profiled reactive astrocytes from mice that were treated with a systemic injection of lipopolysaccharide (LPS), or that received middle cerebral artery occlusion to induce ischaemia[5]. We found that neuroinflammation and ischaemia induced two different types of reactive astrocytes that we termed A1 and A2, respectively (in analogy to the M1/M2 macrophage nomenclature, a nomenclature under current refinement because macrophages can display more than two polarization states[8,9]). A1 astrocytes highly upregulate many classical complement cascade genes previously shown to be destructive to synapses, so we postulated that A1 astrocytes might be harmful. By contrast, A2 astrocytes upregulated many neurotrophic factors, and we therefore postulated that A2 astrocytes were protective. Consistent with this latter possibility, previous studies have provided evidence that reactive astrocytes induced by ischaemia promote CNS recovery and repair[1,10,11].

Here we show that A1 astrocytes are induced by activated microglia. A1 astrocytes lose most normal astrocytic functions but gain a new neurotoxic function, rapidly killing neurons and mature, differentiated oligodendrocytes. We show that A1 astrocytes form rapidly *in vivo* after CNS injury and are present in many human neurodegenerative diseases. Inhibition of A1 astrocyte formation after acute CNS injury prevents death of axotomized neurons. We therefore conclude that A1 astrocytes are harmful, contributing to neuron death after acute CNS injury. Understanding the multidimensional roles of reactive astrocytes has the potential to contribute to the development of new treatment strategies to reduce CNS cell loss and neurological impairment after acute CNS injury as well as in neurodegenerative diseases.

Cellular and molecular inducers of the A1 phenotype

We first investigated whether microglia induce A1 astrocytes, because LPS is a strong inducer of A1 astrocytes[1] and is an activator of TLR4 signalling, a receptor expressed specifically by microglial cells in the rodent CNS[12–15]. We used *Csf1r*$^{-/-}$ knockout mice that lack microglia[16] (Extended Data Fig. 1) to investigate whether A1 astrocytes can be produced without microglia. To assess astrocyte reactivity, we used a microfluidic quantitative (q)PCR screen to determine gene expression changes in astrocytes purified by immunopanning from saline- and LPS-treated wild-type control or *Csf1r*$^{-/-}$ mice. As expected, wild-type littermate controls had a normal response to LPS injection[5,17], with robust induction of an A1 response (Fig. 1a), however *Csf1r*$^{-/-}$ mice

[1]Department of Neurobiology, Stanford University, School of Medicine, Stanford, California 94305, USA. [2]Department of Pharmacology and Therapeutics, University of Melbourne, Parkville, Victoria 3010, Australia. [3]Department of Psychiatry and Behavioral Sciences, Stanford University, School of Medicine, Stanford, California 94305, USA. [4]Eli and Edythe Broad Center of Regeneration Medicine and Stem Cell Research, University of California San Francisco, San Francisco, California 94143, USA. [5]Department of Neurology, Klinikum rechts der Isar, Technical University of Munich, Munich 81675, Germany. [6]Department of Biological Sciences, Korea Advanced Institute of Science and Technology (KAIST), Daejeon 34141, South Korea. [7]Department of Neurology & Neurological Sciences, Stanford University, School of Medicine, Stanford, California 94305, USA. [8]Department of Neurology, F. M. Kirby Neurobiology Center, Boston Children's Hospital, Boston, Massachusetts 02115, USA. [9]Department of Microbiology and Immunology, Stanford University, School of Medicine, Stanford, California 94305, USA. [10]Neuroregeneration and Stem Cell Programs, Institute for Cell Engineering, Johns Hopkins University School of Medicine, Baltimore, Maryland 21205, USA. [11]Department of Neurology, Johns Hopkins University School of Medicine, Baltimore, Maryland 21205, USA. [12]Adrienne Helis Malvin Medical Research Foundation, New Orleans, Louisiana 70130-2685, USA. [13]Departments of Pediatrics and Neurosurgery, University of California San Francisco, San Francisco, California 94143, USA. [14]Department of Paediatrics, University of Cambridge, Cambridge CB2 0AH, UK. [15]Department of Physiology, Johns Hopkins University School of Medicine, Baltimore, Maryland 21205, USA. [16]Solomon H. Snyder Department of Neuroscience, Johns Hopkins University School of Medicine, Baltimore, Maryland 21205, USA. [17]Department of Pharmacology and Molecular Sciences, Johns Hopkins University School of Medicine, Baltimore, Maryland 21205, USA.

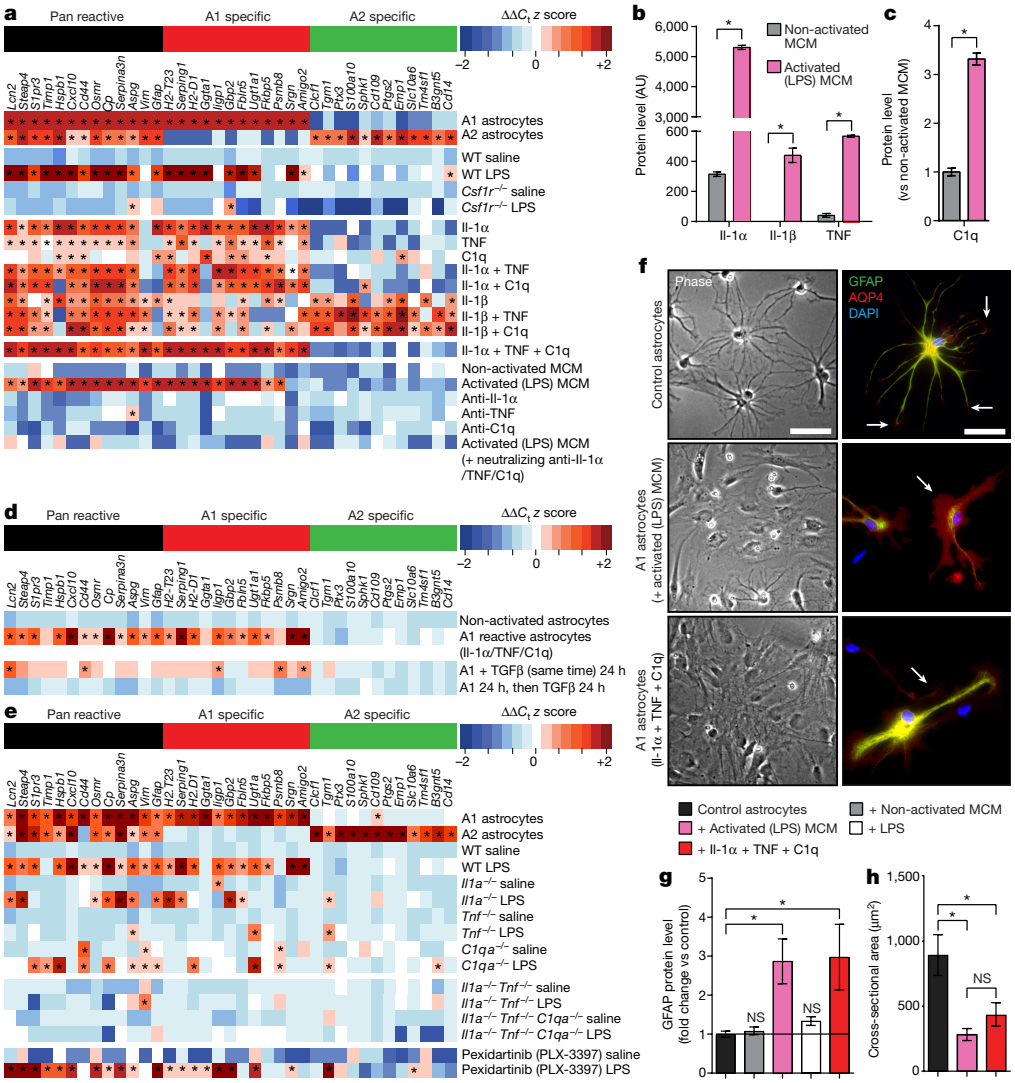

Figure 1 | A serum-free culture model for A1 astrocytes. a, Heat map of reactive transcripts. *Csf1r*$^{-/-}$ mice (which lack microglia) fail to produce A1 astrocytes following LPS injection. LPS-activated microglia, or a combination of Il-1α, TNF and C1q are able to induce A1 astrocytes in culture. WT, wild-type. **b**, Cytokine array analysis of LPS-activated microglia-conditioned medium (MCM) with increases in Il-1α, Il-1β and TNF (Il-1β was not A1-specific). AU, arbitrary units. **c**, Western blot analysis of LPS-activated MCM for C1q protein. **d**, TGFβ was able to reset A1 astrocytes to a non-reactive state. **e**, Individual, single-knockout (*Il1a*$^{-/-}$, *Tnf*$^{-/-}$, *C1qa*$^{-/-}$), double-knockout (*Il1a*$^{-/-}$*Tnf*$^{-/-}$) and triple-knockout (*Il1a*$^{-/-}$*Tnf*$^{-/-}$*C1qa*$^{-/-}$) mice fail to produce A1 astrocytes following LPS injection. Mice treated with pexidartinib (PLX-3397) for 7 days to deplete 95% of microglia (Extended Data Fig. 1) still respond to LPS by producing A1 astrocytes. **f**, Representative phase and fluorescent immunohistochemistry micrographs for GFAP and AQP4 of control and A1 astrocytes. **g**, Western blot analysis of GFAP protein in cultured astrocytes showing an approximate threefold increase in A1 astrocytes compared to control. **h**, Measurements of cross-sectional area of astrocytes stained with GFAP. $n = 6$–8 for each experiment. $^*P < 0.05$; NS, not significant; one-way ANOVA. Data are mean ± s.e.m. Scale bars, 50 μm.

failed to generate A1 astrocytes. These findings show that reactive microglia are required to induce A1 astrocytes *in vivo*.

To determine which microglia-secreted signals induce A1 astrocytes, we next performed a screen to test various candidate molecules individually. We used immunopanning[18] to prepare highly pure populations of resting (non-reactive) astrocytes (Extended Data Fig. 2a, b). We cultured purified astrocytes in serum-free conditions and tested the effects of various molecules on gene expression using our microfluidic assay. As a control, we first investigated if astrocytes in culture can respond to LPS and found that they do not (Extended Data Fig. 2). This was expected, as rodent astrocytes lack receptors and downstream signalling components required for LPS activation (TLR4 and MYD88)[12–14]. We found, however, that several cytokines could induce some, but not all, A1 reactive genes. The strongest inducers of a partial A1 phenotype were interleukin 1α (Il-1α), tumour necrosis factor (TNF), and complement component 1, subcomponent q (C1q). When purified astrocytes were cultured with all three cytokines, astrocytes showed an A1 phenotype nearly identical to the A1 phenotype induced by LPS *in vivo* (Fig. 1a). All three of these cytokines are highly expressed specifically by microglia[13,15], again suggesting a critical role for microglia in inducing A1 astrocytes.

Reactive microglia induce A1 astrocytes

To further confirm that microglia induce A1 astrocytes, we purified microglia by immunopanning. We then cultured astrocytes in non-activated microglia-conditioned medium (MCM) or MCM from microglia that had first been exposed to LPS. We found that LPS-activated MCM, but not non-activated MCM, strongly induced A1 astrocytes (Fig. 1a). The level to which these transcripts were induced was comparable to that seen *in vivo* following systemic LPS injection[5] (Extended Data Fig. 3).

To verify which cytokines microglia use to signal A1 induction, we purified microglia by immunopanning and determined which cytokines were secreted by resting and LPS-activated microglia. Levels

of Il-1α, TNF and C1q were all significantly elevated after microglial activation (Fig. 1b, c). Il-1β secretion also increased in LPS-activated MCM, but was unable to induce expression of A1 transcripts (Fig. 1a). We also tested a range of other microglia-secreted cytokines that were unable to induce A1 astrocytes (Extended Data Fig. 2). The combination of Il-1α, TNF and C1q however, closely mimicked the ability of LPS-reactive MCM (Fig. 1a).

To ensure no other factors secreted by LPS-activated microglia could also generate A1 astrocytes, we collected LPS-activated MCM and pre-treated it with neutralizing antibodies to Il-1α, TNF and C1q. This pre-treated MCM was unable to induce reactive astrocyte genes (Fig. 1a and Extended Data Fig. 3e). Thus Il-1α, TNF and C1q together are sufficient to induce the A1 phenotype, and are necessary for LPS-reactive microglia to induce A1 astrocytes *in vitro*.

We then investigated whether cessation of Il-1α, TNF, and C1q signalling enables A1 astrocytes *in vitro* to revert back to resting astrocytes or whether the A1 phenotype is stable. We removed all three cytokines from A1 cultures, and added neutralizing antibodies to all three to make sure they were fully inhibited. After seven days, we assessed the levels of A1 transcripts and found that the A1 phenotype remained. Furthermore, we also investigated if additional molecules could revert A1 astrocytes to a non-reactive phenotype. We tested the anti-inflammatory cytokine TGFβ or FGF (as it has previously been shown that astrocyte activation is suppressed in the injured brain by FGF signalling[19]). We grew A1 astrocytes in culture, then treated them with TGFβ or FGF and found both significantly decreased reactive astrocyte transcript levels (Fig. 1d and Extended Data Fig. 3). Whether or not there are additional signalling processes that can revert A1 astrocytes *in vivo* is an important question for future studies.

We next investigated if genetic deficiency of Il-1α, TNF or C1q would be sufficient to prevent A1 astrocyte reactivity *in vivo*. First we checked if single-knockout mice (*Il1a*$^{-/-}$, *Tnf*$^{-/-}$, or *C1qa*$^{-/-}$) were still able to produce neuroinflammatory reactive microglia following systemic LPS injection. Using qPCR we observed that microglia from these animals still had many reactive transcripts[15] that were highly upregulated 24 h after LPS injection (Extended Data Fig. 4). We next used astrocytes purified from these same mice and used our microfluidic qPCR screen to determine whether the cells were reactive. Each knockout mouse had significantly decreased A1 astrocyte reactivity (Fig. 1e). Additionally, we investigated double-knockout (*Il1a*$^{-/-}$*Tnf*$^{-/-}$) and triple-knockout mice (*Il1a*$^{-/-}$*Tnf*$^{-/-}$*C1qa*$^{-/-}$) and observed decreased A1 reactivity in both, with triple-knockout animals having no reactive response following systemic LPS injection (Fig. 1e). Microglia from these same knockout mice still upregulated inflammatory mediators in response to LPS injection, but simply failed to release A1 initiators (Extended Data Fig. 4). Taken together our data show that microglia-derived Il-1α, TNF and C1q work together to mediate A1 astrocyte induction.

A1 astrocytes lose many normal astrocytic functions

Next we investigated whether A1 astrocytes are able to induce the formation of functional synapses *in vitro*. We cultured purified retinal ganglion cells (RGCs) with resting or A1 astrocytes and quantified synapse number by double immunostaining for pre- and postsynaptic proteins (Fig. 2a and Extended Data Fig. 5). RGCs cultured with A1 astrocytes had 50% less synapses compared to those grown with resting astrocytes (Fig. 2b). When RGCs were cultured with resting astrocytes to induce synapse formation and then cultured with A1 astrocytes, synapse number significantly decreased by about 40%, suggesting that A1 astrocytes are either unable to maintain these synapses or actively disassemble them.

Astrocytes induce the formation of excitatory synapses by secreting glypicans (GPC4 and GPC6 (ref. 20)), SPARCL1 (ref. 21) and thrombospondins (THBS1 and THBS2)[22], so we next investigated whether reactive astrocytes still produce these factors. Quantitative PCR showed decreased expression of *Gpc6* and *Sparcl1*, while simultaneously showing increased expression of *Thbs1* and *Thbs2* (Fig. 2c). This increase in thrombospondins, which should increase synaptic number, suggests that the decreased synapse number may reflect an A1-induced toxicity to synapses (see below). To determine the effects of A1 astrocytes on synapse function we used whole-cell patch-clamp recording on RGCs cultured with resting astrocytes or A1 astrocytes. RGCs cultured with A1 astrocytes had significantly decreased frequency and amplitude of miniature excitatory postsynaptic currents when compared to RGCs cultured with resting astrocytes (Fig. 2d–g).

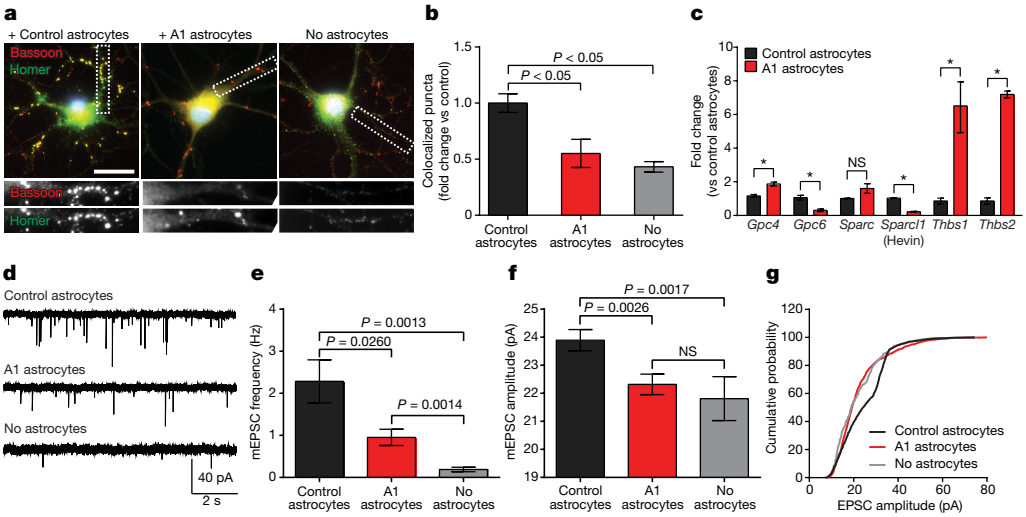

Figure 2 | A1 astrocytes do not promote synapse formation or function. **a**, Representative images of retinal ganglion cells (RGCs) grown without astrocytes, or with control or A1 astrocytes, immunostained with pre- and postsynaptic markers homer (green) and bassoon (red). Co-localization (yellow puncta) was counted as a structural synapse. **b**, Total number of synapses normalized per each individual RGC, $n = 50$ neurons in each treatment. **c**, Quantitative PCR for astrocyte-secreted, synaptogenic factors. **d**, Representative traces of whole-cell patch-clamp miniature excitatory postsynaptic current (mEPSC) recordings from RGCs. **e**, Frequency of mEPSCs was significantly decreased in the presence of A1 astrocytes (RGCs without astrocytes, 0.19 ± 0.05 Hz, $n = 12$ neurons; RGCs with resting astrocytes, 2.28 ± 0.51 Hz, $n = 14$ neurons; RGCs with A1 astrocytes, 0.95 ± 0.19 Hz, $n = 16$ neurons). **f**, A1 astrocytes significantly decreased the mean amplitude of mEPSCs (RGCs without astrocytes, 21.81 ± 0.78 pA, $n = 12$ neurons; RGCs with resting astrocytes, 23.89 ± 0.38 pA $n = 14$ neurons; RGCs with A1 astrocytes, 22.32 ± 0.37 pA, $n = 16$ neurons). **g**, RGCs cultured with A1 astrocytes had significantly more small-amplitude mEPSCs in cumulative probability histograms ($P < 0.0001$ Kolmogorov–Smirnov test, $n = 12$–16 neurons per condition). *$P < 0.05$, one-way ANOVA. Data are mean ± s.e.m. Scale bar, 10 μm.

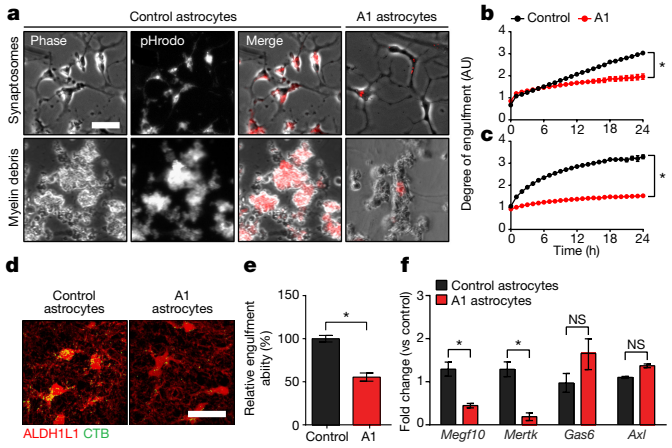

Figure 3 | A1 astrocytes lose phagocytic capacity. a–c, Phase and fluorescence images of cultured astrocytes engulfing pHrodo-conjugated synaptosomes (quantification in **b**) and myelin debris (quantification in **c**). **d**, **e**, Representative confocal reconstruction (**d**) and quantification (**e**) showing cholera toxin B (CTB)-labelled retinal ganglion cell projections engulfed by control and A1 astrocytes in the dorsal lateral geniculate nucleus. $n = 4$ per group. **f**, Quantitative PCR analysis of astrocyte-specific phagocytic receptors (*Megf10* and *Mertk*, decreased in A1 astrocytes) and bridging molecules (*Gas6* and *Axl*, unchanged). $^*P < 0.05$; NS, not significant; one-way ANOVA, or Student's *t*-test as appropriate. Data are mean ± s.e.m. Scale bars, 15 μm (**a**) and 10 μm (**d**).

Taken together, these results show that A1 astrocytes induce the formation of fewer synapses, and the few synapses they do induce are significantly weaker when compared to those produced by healthy resting astrocytes.

To compare phagocytic ability of control and A1 astrocytes, we measured engulfment of purified synaptosomes. A1 astrocytes engulfed 50–75% fewer synaptosomes than control astrocytes (Fig. 3a, b). Similarly, we found that control astrocytes are able to robustly phagocytose myelin debris, but upon conversion to an A1 phenotype, astrocytes almost completely lose this capacity (Fig. 3a, c). This phagocytic deficit corresponded with a 90% decrease in *Mertk* and 60% decrease in *Megf10* mRNA, phagocytic receptors we have previously found to mediate synaptic phagocytosis[3] (Fig. 3f). To determine whether A1 astrocytes also display decreased phagocytic ability *in vivo*, we used *Aldh1l1–eGFP* transgenic mice and LPS injection (Extended Data Fig. 6) to visualize phagocytosis of Alexa594-conjugated cholera toxin-β (CTB-594)-labelled synapses by control and A1 astrocytes. Confocal microscopy was used to visualize engulfed CTB-labelled synapses inside *Aldh1l1–eGFP* fluorescent astrocytes as previously reported[3]. We found that A1 astrocytes in the lateral geniculate nucleus *in vivo* show the same significant loss of synaptic engulfment ability (around 50% compared to astrocytes in saline-treated control animals) as was seen in our *in vitro* assay (Fig. 3a, b, d, e). Combined, these data show that A1 astrocytes have deficiencies in phagocytosis of both synaptosomes and myelin debris in culture, that this deficiency can also influence efficiency of synaptic pruning *in vivo*, and suggest that A1 astrocytes may well lose the capacity to clear myelin debris *in vivo*, an important area for future investigation.

A1 astrocytes are powerfully neurotoxic

Normally astrocytes promote CNS neuronal survival[23]. To determine whether A1 astrocytes also promote neuronal survival, we co-cultured control and A1 astrocytes with purified RGCs and measured viability. We found that RGCs rapidly died when grown with increasing concentrations of A1-astrocyte-conditioned medium (Fig. 4a, c). At the highest concentrations there was almost 100% cell death (Fig. 4c). A1 astrocytes were similarly toxic to cortical neurons, embryonic spinal motor neurons and mature, differentiated oligodendrocytes (Fig. 4b, d); however, even at high doses spinal motor neurons remained around 20% viable. We also found that preganglionic and gamma motor neurons were not susceptible to A1-induced toxicity (Extended Data Fig. 7m). Although not toxic to oligodendrocyte precursor cells, A1 astrocytes were able to slow their differentiation and division (Extended Data Fig. 8). In addition, we tested the susceptibility of human dopaminergic neurons to A1-induced toxicity and found that, like rodent cells, they also showed decreased viability, with 25% of human dopaminergic cells dying as a result of A1-induced toxicity (Fig. 4e). This death could not be attributed to Il-1α, TNF and C1q alone, which did not cause cell death in purified cultures. Death was blocked by caspase-2 and caspase-3 inhibitors but not by necrostatin or glutamate blockers and thus appeared to be due to apoptosis (Extended Data Fig. 9). These results suggest that A1 astrocytes secrete a soluble toxin that rapidly kills a subset of CNS neurons and mature oligodendrocytes, but not other CNS cell types.

A1 astrocytes kill axotomized CNS neurons

Why CNS neurons die after axotomy has long remained an unanswered question. One idea is that axotomy interrupts a retrograde neurotrophic signal. Because injured spinal cords contain neuroinflammatory microglia and/or macrophages[24], we hypothesized that axotomy could also induce formation of A1 astrocytes which in turn kill axotomized neurons. We used optic nerve crush (ONC) in postnatal rats and mice as a model system. ONC rapidly induced robust A1 generation that was temporally paired with death of RGCs (Fig. 4i–o). Weekly injection of neutralizing antibodies to Il-1α, TNF and C1q into the vitreous of the eye from the time of injury inhibited A1 formation and prevented death of RGCs for at least 14 days after ONC (Fig. 4g–j). Finally, we performed ONC in double-knockout ($Il1a^{-/-}Tnf^{-/-}$) and triple-knockout ($Il1a^{-/-}Tnf^{-/-}C1qa^{-/-}$) mice that fail to generate A1 astrocytes, and found that seven days after ONC RGCs remained viable, unlike wild-type control mice (Fig. 4k). These data provide strong evidence that death of RGCs after axotomy is not as a result of trophic deprivation but is instead due to release of a toxic signal from nearby neurotoxic A1 astrocytes.

A1 astrocytes in human disease

Because A1 astrocytes are induced after injury and by LPS (a well-described neurodegeneration sensitizer that causes extensive neuroinflammation[25,26]), and because reactive microglia are found in neurodegenerative diseases, we investigated whether A1 astrocytes are present in human neuroinflammatory and neurodegenerative diseases. Because complement component 3 (*C3*) is one of the most characteristic and highly upregulated genes in A1 astrocytes and is not expressed by ischaemic A2 reactive astrocytes (Extended Data Fig. 10), we carried out *in situ* hybridization and immunochemistry on post-mortem tissue from patients with Alzheimer's disease (AD), Huntington's disease, Parkinson's disease, amyotrophic lateral sclerosis, and multiple sclerosis (MS) to identify whether there are C3-expressing A1 astrocytes in these diseases. We found many GFAP- and S100β-positive astrocytes that were C3-positive (either by *in situ* hybridization or immunofluorescence) in regions traditionally associated with each disease (Fig. 5), and qPCR analysis confirmed upregulation of *C3* in post-mortem tissue samples. In demyelinating lesions of MS, C3-positive astrocytes were typically closely associated with CD68-positive activated microglia and/or macrophages (Fig. 5 and Extended Data Fig. 11). In human AD, nearly 60% of GFAP-positive astrocytes in the prefrontal cortex were positive for C3, suggesting that A1 astrocytes make up a large proportion of astrocytes in AD in the CNS regions that are affected by neurodegeneration, and may thus be integral for disease initiation and progression. In addition to C3, reactive astrocytes in these diseases were also immunoreactive for several other A1-specific markers (Extended Data Fig. 11). These findings demonstrate that A1-like reactive astrocytes are present in most major neurodegenerative diseases, raising the possibility that they help to drive neurodegeneration.

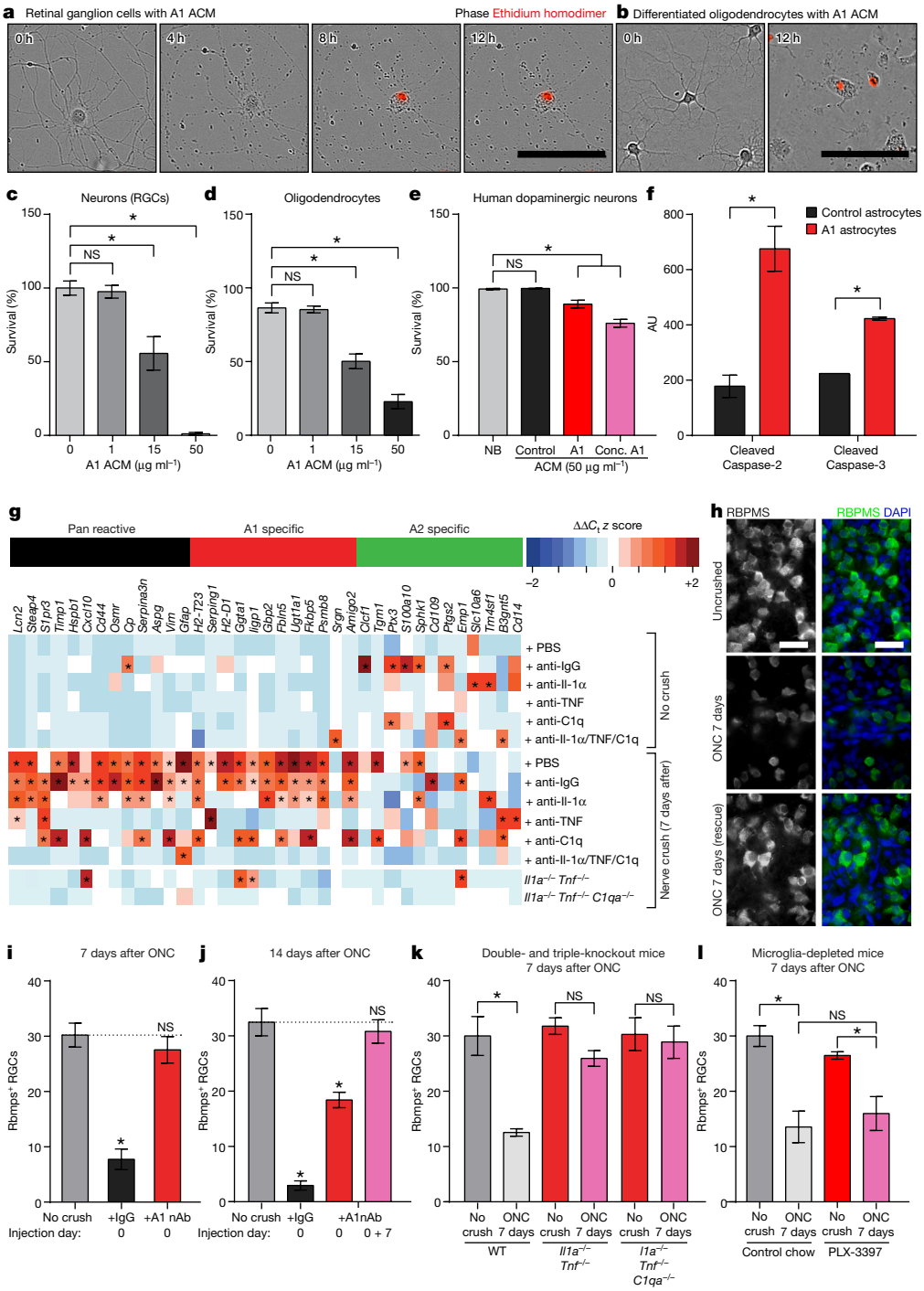

Figure 4 | An astrocyte-derived toxic factor promoting cell death. **a**–**d**, Representative phase images showing the death of purified retinal ganglion cells (RGCs) in culture (ethidium homodimer stain in red shows DNA in the dead cells (**a**, 24 h quantification in **c**), and differentiated oligodendrocytes (**b**, 24 h quantification in **d**). **e**, Quantification of A1-induced cell death in human dopaminergic neurons (5 days). NB, neurobasal media control. **f**, Western blot analysis for cleaved caspase-2 and caspase-3 in RGCs treated with control or A1-astrocyte-conditioned medium. **g**, Retro-orbital optic nerve crushes (ONC) induced A1 astrocytes in the retina. Intravitreal injection of neutralizing antibodies to Il-1α, TNF and C1q blocked A1 production. **h**, Rbpms (RNA-binding protein with multiple splicing, an RGC marker) immunostaining of whole-mount retinas showed decreased number of RGCs in ONC, which were rescued with neutralizing antibody treatment (A1 nAb). **i**–**l**, Quantification is shown after ONC at 7 days (**i**), 14 days (**j**) using neutralizing antibodies, and at 7 days using *Il1a*$^{-/-}$*TNF*$^{-/-}$ and *Il1a*$^{-/-}$*TNF*$^{-/-}$*C1qa*$^{-/-}$ animals (**k**), and microglia-depleted (PLX-3397-treated) animals (**l**). *$P < 0.05$, one-way ANOVA ($n = 8$). Data are mean ± s.e.m. Scale bars, 100 μm (**a**, **b**) and 20 μm (**h**).

Concluding remarks

Here we identify neurotoxic, reactive, A1 astrocyte formation as a fundamental pathological response of the CNS to LPS-induced neuroinflammation, acute CNS injury and many neurodegenerative diseases. Our findings indicate a role for activated microglia in inducing A1 astrocytes via secretion of Il-1α, TNF and C1q *in vitro* and *in vivo*. In contrast to A2 reactive astrocytes, which are induced by ischaemia[5] and strongly promote neuronal survival and tissue repair[10,27–29], A1 astrocytes secrete a neurotoxin that induces rapid death of neurons and oligodendrocytes. A1 astrocytes have lost many characteristic

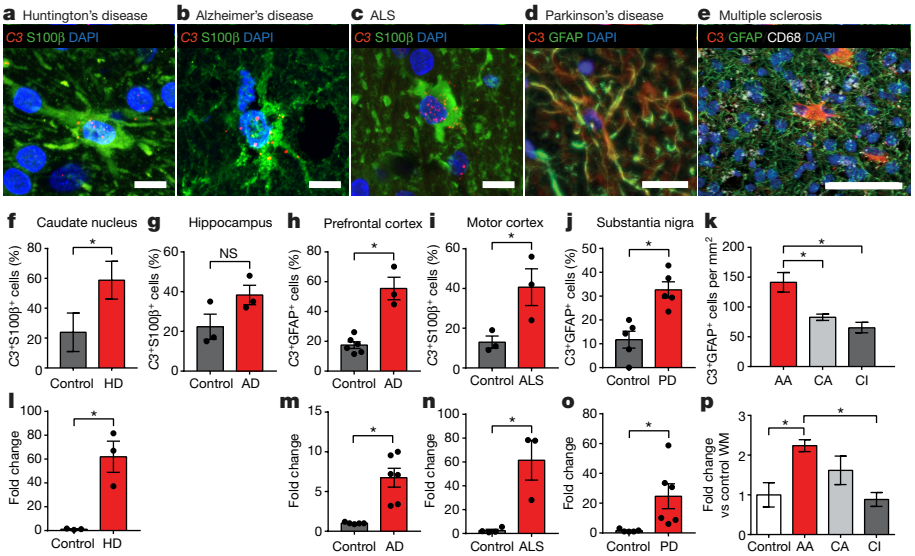

Figure 5 | A1 (C3-positive) reactive astrocytes in human disease. **a**–**e**, Representative *in situ* hybridization for *C3* and immunofluorescence staining for S100β in Huntington's (HD, **a**) and Alzheimer's (AD, **b**) diseases, and amyotrophic lateral sclerosis (ALS, **c**), and co-immunofluorescence staining for C3 and GFAP in Parkinson's disease (PD, **d**) and multiple sclerosis (MS, **e**). **f**–**k**, Quantification in HD (**f**); AD in both hippocampus (**g**) and prefrontal cortex (**h**); ALS (**i**), PD (**j**) and MS (**k**) shows that around 30–60% of astrocytes in brain regions specific to each disease in humans are C3-positive A1 astrocytes. WM, white matter; AA, acute active demyelinating lesion; CA, chronic active demyelinating lesion; CI, chronic inactive demyelinated lesion. **l**–**p**, Increase in expression of *C3* transcript in all diseases (by qPCR). $n = 3$–8 disease and 5–8 control samples in each instance. Quantification was carried out on 5 fields of view and approximately 50 cells were surveyed per sample. Scale bars, 100 μm (**e**), 20 μm (**d**), 10 μm (**a**–**c**). Data are mean ± s.e.m. $^*P < 0.05$, Student's *t*-test (**f**–**j**, **l**–**o**), one-way ANOVA (**k**, **p**) compared to age-matched control.

astrocytic functions, including the ability to promote neuronal survival and outgrowth, promote synapse formation and function, and to phagocytose synapses and myelin debris. A1 astrocytes are rapidly induced after acute CNS injury and responsible for the death of axotomized RGCs. A1 astrocytes are also abundant in neurodegenerative diseases, where their presence may well contribute to neurodegeneration and help to drive disease progression.

These findings raise important questions. Perhaps most importantly, what is the identity of the neurotoxin? We are currently using biochemical approaches in an attempt to purify and characterize it. Also, to what extent are A1 astrocytes present in spinal cord injury, CNS brain trauma and other neuroinflammatory and neurodegenerative diseases, and are A1 astrocytes actively driving the death of neurons, axons, and synapses and/or oligodendrocytes in these diseases? Astrocytes have been found to be toxic to spinal motor neurons in ALS[30,31]—do these astrocytes have an A1 phenotype? In AD, oligomeric amyloid-β is a strong activator of microglia[32] and our findings provide evidence that A1 astrocytes are present in regions of neurodegeneration in human post-mortem tissue. Although we found that activated microglia were insufficient by themselves to kill neurons, they strongly induce A1 astrocytes, which could drive neurodegeneration not only by secreting a neurotoxin but also by releasing multiple complement components that help to drive synapse degeneration[33]. In acute relapsing and remitting MS, we also observed C3-expressing A1 astrocytes in demyelinating plaques. This suggests the possibility that demyelinating lesions, which generally also contain unmyelinated axons and oligodendrocyte precursor cells, fail to remyelinate because A1 astrocytes inhibit oligodendrocyte precursor cell proliferation and differentiation, and kill any newly generated oligodendrocytes (in the chronic progressive phase of the disease A1 astrocytes might also drive axon degeneration). Would drugs that prevent or revert A1 formation or block the action of the A1 neurotoxin prevent neurodegeneration in these diseases, and stimulate spontaneous remyelination in MS and new synapse formation in diseases such as AD? Similarly, would drugs that prevent or revert A1 astrocytes save axotomized CNS neurons after spinal cord injury and promote regeneration by stimulating growth and allowing these astrocytes to clear myelin debris? Future studies should test these possibilities in animal models, as antibody therapies that inhibit human IL-1α and TNF are already FDA-approved and in use for other medical conditions. Lastly, it may be of interest to investigate whether epithelial cells outside the CNS undergo an A1-like neurotoxic transformation after injury or disease that contributes to the death of non-CNS cell types, such as β islet cells in diabetes.

A noteworthy question raised by our findings is why the injured and diseased CNS would produce a neurotoxic, reactive astrocyte. A1 astrocytes might remove dysfunctional neurons to help preserve neuron circuit function, or they might help to fight off infections. Although A1 astrocytes are not directly toxic to bacteria, they do secrete many complement cascade components that are expected to greatly enhance the clearance of bacteria by the immune system. Similarly, they may kill virally infected neurons in order to prevent the spread of viruses, or modify CNS immune responses by killing specific types of infiltrating immune cells. Whatever the answers, new drugs that prevent A1 formation, promote A1 reversion or block the A1 neurotoxin hold great potential to treat a variety of chronic neurological diseases and acute CNS injuries.

Online Content Methods, along with any additional Extended Data display items and Source Data, are available in the online version of the paper; references unique to these sections appear only in the online paper.

Received 6 May; accepted 28 November 2016.
Published online 18 January 2017.

1. Sofroniew, M. V. & Vinters, H. V. Astrocytes: biology and pathology. *Acta Neuropathol.* **119,** 7–35 (2010).
2. Clarke, L. E. & Barres, B. A. Emerging roles of astrocytes in neural circuit development. *Nat. Rev. Neurosci.* **14,** 311–321 (2013).
3. Chung, W.-S. S. *et al.* Astrocytes mediate synapse elimination through MEGF10 and MERTK pathways. *Nature* **504,** 394–400 (2013).
4. Liddelow, S. & Barres, B. SnapShot: astrocytes in health and disease. *Cell* **162,** 1170–1170.e1 (2015).
5. Zamanian, J. L. *et al.* Genomic analysis of reactive astrogliosis. *J. Neurosci.* **32,** 6391–6410 (2012).
6. Anderson, M. A. *et al.* Astrocyte scar formation aids central nervous system axon regeneration. *Nature* **532,** 195–200 (2016).
7. Sofroniew, M. V. Astrogliosis. *Cold Spring Harb. Perspect. Biol.* **7,** a020420 (2014).
8. Martinez, F. O. & Gordon, S. The M1 and M2 paradigm of macrophage activation: time for reassessment. *F1000Prime Rep.* **6,** 13 (2014).
9. Heppner, F. L., Ransohoff, R. M. & Becher, B. Immune attack: the role of inflammation in Alzheimer disease. *Nat. Rev. Neurosci.* **16,** 358–372 (2015).

10. Bush, T. G. *et al.* Leukocyte infiltration, neuronal degeneration, and neurite outgrowth after ablation of scar-forming, reactive astrocytes in adult transgenic mice. *Neuron* **23,** 297–308 (1999).
11. Zador, Z., Stiver, S., Wang, V. & Manley, G. T. Role of aquaporin-4 in cerebral edema and stroke. *Handb. Exp. Pharmacol.* **190,** 159–170 (2009).
12. Cahoy, J. D. *et al.* A transcriptome database for astrocytes, neurons, and oligodendrocytes: a new resource for understanding brain development and function. *J. Neurosci.* **28,** 264–278 (2008).
13. Zhang, Y. *et al.* An RNA-sequencing transcriptome and splicing database of glia, neurons, and vascular cells of the cerebral cortex. *J. Neurosci.* **34,** 11929–11947 (2014).
14. Zhang, Y. *et al.* Purification and characterization of progenitor and mature human astrocytes reveals transcriptional and functional differences with mouse. *Neuron* **89,** 37–53 (2016).
15. Bennett, M. L. *et al.* New tools for studying microglia in the mouse and human CNS. *Proc. Natl Acad. Sci. USA* **113,** E1738–E1746 (2016).
16. Ginhoux, F. *et al.* Fate mapping analysis reveals that adult microglia derive from primitive macrophages. *Science* **330,** 841–845 (2010).
17. Cartmell, T., Luheshi, G. N. & Rothwell, N. J. Brain sites of action of endogenous interleukin-1 in the febrile response to localized inflammation in the rat. *J. Physiol. (Lond.)* **518,** 585–594 (1999).
18. Foo, L. C. *et al.* Development of a method for the purification and culture of rodent astrocytes. *Neuron* **71,** 799–811 (2011).
19. Kang, W. *et al.* Astrocyte activation is suppressed in both normal and injured brain by FGF signaling. *Proc. Natl Acad. Sci. USA* **111,** E2987–E2995 (2014).
20. Allen, N. J. *et al.* Astrocyte glypicans 4 and 6 promote formation of excitatory synapses via GluA1 AMPA receptors. *Nature* **486,** 410–414 (2012).
21. Kucukdereli, H. *et al.* Control of excitatory CNS synaptogenesis by astrocyte-secreted proteins Hevin and SPARC. *Proc. Natl Acad. Sci. USA* **108,** E440–E449 (2011).
22. Christopherson, K. S. *et al.* Thrombospondins are astrocyte-secreted proteins that promote CNS synaptogenesis. *Cell* **120,** 421–433 (2005).
23. Banker, G. A. Trophic interactions between astroglial cells and hippocampal neurons in culture. *Science* **209,** 809–810 (1980).
24. Kigerl, K. A. *et al.* Identification of two distinct macrophage subsets with divergent effects causing either neurotoxicity or regeneration in the injured mouse spinal cord. *J. Neurosci.* **29,** 13435–13444 (2009).
25. Castaño, A., Herrera, A. J., Cano, J. & Machado, A. Lipopolysaccharide intranigral injection induces inflammatory reaction and damage in nigrostriatal dopaminergic system. *J. Neurochem.* **70,** 1584–1592 (1998).
26. Liu, Y. *et al.* Dextromethorphan protects dopaminergic neurons against inflammation-mediated degeneration through inhibition of microglial activation. *J. Pharmacol. Exp. Ther.* **305,** 212–218 (2003).
27. Faulkner, J. R. *et al.* Reactive astrocytes protect tissue and preserve function after spinal cord injury. *J. Neurosci.* **24,** 2143–2155 (2004).
28. Okada, S. *et al.* Conditional ablation of Stat3 or Socs3 discloses a dual role for reactive astrocytes after spinal cord injury. *Nat. Med.* **12,** 829–834 (2006).
29. Herrmann, J. E. *et al.* STAT3 is a critical regulator of astrogliosis and scar formation after spinal cord injury. *J. Neurosci.* **28,** 7231–7243 (2008).
30. Di Giorgio, F. P., Boulting, G. L., Bobrowicz, S. & Eggan, K. C. Human embryonic stem cell-derived motor neurons are sensitive to the toxic effect of glial cells carrying an ALS-causing mutation. *Cell Stem Cell* **3,** 637–648 (2008).
31. Nagai, M. *et al.* Astrocytes expressing ALS-linked mutated SOD1 release factors selectively toxic to motor neurons. *Nat. Neurosci.* **10,** 615–622 (2007).
32. Reed-Geaghan, E. G., Savage, J. C., Hise, A. G. & Landreth, G. E. CD14 and toll-like receptors 2 and 4 are required for fibrillar Abeta-stimulated microglial activation. *J. Neurosci.* **29,** 11982–11992 (2009).
33. Stevens, B. *et al.* The classical complement cascade mediates CNS synapse elimination. *Cell* **131,** 1164–1178 (2007).

Supplementary Information is available in the online version of the paper.

Acknowledgements We thank R. Vance (UC Berkeley) for gifting *Il-1α*$^{-/-}$ mice and E. R. Stanley (Albert Einstein College of Medicine) for gifting *Csf1r*$^{-/-}$ mice. This work was supported by grants from the National Institutes of Health (R01 AG048814, B.A.B.; RO1 DA15043, B.A.B.; P50 NS38377, V.L.D. and T.M.D.) Christopher and Dana Reeve Foundation (B.A.B.), the Novartis Institute for Biomedical Research (B.A.B.), Dr. Miriam and Sheldon G. Adelson Medical Research Foundation (B.A.B.), the JPB Foundation (B.A.B., T.M.D.), the Cure Alzheimer's Fund (B.A.B.), the Glenn Foundation (B.A.B.), the Esther B O'Keeffe Charitable Foundation (B.A.B.), the Maryland Stem Cell Research Fund (2013-MSCRFII-0105-00, V.L.D.; 2012-MSCRFII-0268-00, T.M.D.; 2013-MSCRFII-0105-00, T.M.D.; 2014-MSCRFF-0665, M.K.). S.A.L. was supported by a postdoctoral fellowship from the Australian National Health and Medical Research Council (GNT1052961), and the Glenn Foundation Glenn Award. L.E.C. was funded by a Merck Research Laboratories postdoctoral fellowship (administered by the Life Science Research Foundation). W.-S.C. was supported by a career transition grant from NEI (K99EY024690). C.J.B. was supported by a postdoctoral fellowship from Damon Runyon Cancer Research Foundation (DRG-2125-12). L.S. was supported by a postdoctoral fellowship from the German Research Foundation (DFG, SCHI 1330/1-1). T.M.D. is the Leonard and Madlyn Abramson Professor in Neurodegenerative Diseases. The authors (N.P., M.K., V.L.D. and T.M.D.) acknowledge the joint participation by the Adrienne Helis Malvin Medical Research Foundation through its direct engagement in the continuous active conduct of medical research in conjunction with The Johns Hopkins Hospital and the Johns Hopkins University School of Medicine and the Foundation's Parkinson's Disease Program M-2014. We thank the Stanford Alzheimer's disease research Centre (AG047366), the Stanford Health Care Brain Bank, The Arizona Ageing & Disability Resource Centers (AG019610) and Banner Sun Health for providing control and AD brain samples. We thank R. Reynolds and D. Gveric for providing control and MS brain samples from the UK Multiple Sclerosis Tissue Bank, funded by the Multiple Sclerosis Society of Great Britain and Northern Ireland (registered charity 207495). We would like to thank O. Pletnikova and J. C. Troncoso from the Department of Pathology, Johns Hopkins University School of Medicine, for providing control and PD human sections. We thank the Neurological Foundation of New Zealand Human Brain Bank at the University of Auckland for Control and HD tissue sections for IHC analysis. We thank R. Myers at Boston University Medical Centre for control and HD tissue for q-RTPCR analysis. We thank J. Trojanoswki at the University of Pennsylvania Institute on Aging for AD and ALS tissue samples for in situ analysis. We thank A. Mosberger and A. Rosenthal for careful review of the manuscript. We thank T. Jessell and T. Maniatis for their insightful discussions on motor neuron subtypes. We thank V. and S. Coates for their generous support.

Author Contributions S.A.L. and B.A.B. designed the experiments and wrote the paper. All authors reviewed and edited the manuscript. S.A.L. performed experiments and analysed data. K.G. performed proliferation assays and single-cell analysis. L.E.C. performed and analysed electrophysiology recordings and W.-S.C. performed and analysed *in vivo* astrocyte synapse pruning experiments. M.L.B. and S.A.L. performed optic nerve crushes. B.A.N. performed and analysed bacterial experiments. F.C.B. performed and analysed FACS experiments. T.C.P. performed stroke (MCAO) experiments. C.J.B. developed microglia culture systems. N.P. and M.K. differentiated hES cells to dopaminergic neurons for toxicity assays. Immunohistochemistry and analysis of human tissue was performed by L.S. (MS samples), S.A.L., D.K.W. and A.F. (AD), D.K.W. and A.F. (HD and ALS samples), and N.P. and M.K. (PD samples). qPCR analysis of human tissue was performed by S.A.L. (AD, HD, ALS and PD samples) and L.S. (MS samples). A.E.M. and K.G. provided technical support.

Author Information Reprints and permissions information is available at www.nature.com/reprints. The authors declare competing financial interests: details are available in the online version of the paper. Readers are welcome to comment on the online version of the paper. Correspondence and requests for materials should be addressed to S.A.L. (liddelow@stanford.edu).

Reviewer Information *Nature* thanks M. Freeman, S. Koizumi and the other anonymous reviewer(s) for their contribution to the peer review of this work.

METHODS

Data reporting. All procedures were conducted in accordance with the animal care standards of the National Institute of Health and approved by Stanford University's Administrative Panel on Laboratory Animal Care. Astrocytes and all other CNS cells were purified from postnatal day (P)5 rat or mouse cortex and cultured in serum-free conditions. All experiments with mutants were performed blindly without knowledge of their genotype.

Animals. Sprague Dawley rats were from Charles River. *TNF*$^{-/-}$ (B6.129S–Tnftm1Gkl/J) transgenic mice and wild-type C57BL/6J mice were from Jackson Laboratories. *C1qa*$^{-/-}$ (C57BL/6) were from previous studies in our laboratory[34]. *Il1a*$^{-/-}$ mice were a gift from R. E. Vance. *Tg(Aldh1l1–eGFP)OFC789Gsat/Mmucd* mice were used to visualize astrocytes in *in vivo* phagocytic assays. Double-knockout (*Il1a*$^{-/-}$*TNF*$^{-/-}$) and triple-knockout (*Il1a*$^{-/-}$*TNF*$^{-/-}$*C1qa*$^{-/-}$) animals were developed in house. All lines were maintained by breeding with C57BL/6 mice. Animals were randomly assigned numbers and evaluated thereafter blind (to both experimental condition and genotype).

Immunopanning and cell culture. Astrocytes were purified by immunopanning from P5 rats or mice (see above) forebrains and cultured as previously described[18]. In brief, cortices were enzymatically (using papain) then mechanically dissociated to generate a single-cell suspension that was incubated on successive negative immunopanning plates to remove microglia, endothelial cells and oligodendrocyte lineage cells before positively selecting for astrocytes with an Itgb5-coated panning plate. Isolated astrocytes were cultured in a defined, serum-free base medium containing 50% neurobasal, 50% DMEM, 100 U ml^{-1} penicillin, 100 μg ml^{-1} streptomycin, 1 mM sodium pyruvate, 292 μg ml^{-1} L-glutamine, 1× SATO and 5 μg ml^{-1} of *N*-acetyl cysteine. This medium was supplemented with the astrocyte-required survival factor HBEGF (Peprotech, 100-47) at 5 ng ml^{-1} as previously described[18]. A similar immunopanning protocol was used for other central nervous system cell types, with positive selection using THY1 (cortical neurons), 192 hybridoma clone (embryonic spinal motor neurons[35]), CD31 (endothelial cells[36]), O4 (oligodendrocyte lineage cells), PDGFRβ (pericytes[37]) or CD45 (microglia/macrophages). A1 astrocytes were generated *in vitro* by growing purified astrocytes for 6 days and then treating for 24 h with Il-1α (3 ng ml^{-1}, Sigma, I3901), TNF (30 ng ml^{-1}, Cell Signaling Technology, 8902SF) and C1q (400 ng ml^{-1}, MyBioSource, MBS143105).

Microfluidic qPCR (pooled cell samples). Total RNA was extracted from immunopanned cells using the RNeasy Plus kit (Qiagen) and cDNA synthesis performed using the SuperScript VILO cDNA synthesis kit (Invitrogen) according to supplier protocols. We designed primers using NCBI primer BLAST software (http://www.ncbi.nlm.nih.gov/tools/primer-blast/) and selected primer pairs with least probability of amplifying non-specific products as predicted by NCBI primer BLAST. All primers had 90–105% efficiency. We designed primer pairs to amplify products that spanned exon–exon junctions to avoid amplification of genomic DNA. We tested the specificity of the primer pairs by PCR with rat and mouse whole-brain cDNA (prepared fresh), and examined PCR products by agarose gel electrophoresis. For microfluidic qPCR, 1.25 μl of each cDNA sample was pre-amplified using 2.5 μl of 2× Taqman pre-amplification master mix (Applied Biosystems) and 1.25 μl of the primer pool (0.2 pmol each primer per μl, primer sequences for rat and mouse are provided in Supplementary Tables 1, 2). Pre-amplification was performed using a 10 min 95 °C denaturation step and 14 cycles of 15 s at 95 °C and 4 min at 60 °C. Reaction products were diluted 5× in TE Buffer (Teknova). Five microlitres from a sample mix containing pre-amplified cDNA and amplification Master mix (20 mM $MgCl_2$, 10 mM dNTPs, FastStart Taq polymerase, DNA-binding dye loading reagent, 50× ROX, 20× Evagreen) was loaded into each sample inlet of a 96.96 Dynamic Array chip (Fluidigm Corporation) and 5 μl from an assay mix containing DNA-assay loading reagent, as well as forward and reverse primers (10 pmol μl^{-1}) was loaded into each detector inlet. The chip was then placed in the NanoFlexTM 4-IFC Controller (Fluidigm) for loading and mixing. After loading, the chip was processed in the BioMark Real-Time PCR System (Fluidigm) using a cycling program of 10 min at 95 °C followed by 40 cycles of 95 °C for 15 s, 60 °C for 30 s and 72 °C for 30 s. After completion of qPCR, a melting curve of amplified products was determined. Data were collected using BioMark Data Collection Software 2.1.1 build 20090519.0926 (Fluidigm) as the cycle of quantification (C_q), where the fluorescence signal of amplified DNA intersected with background noise. Fluidigm data were corrected for differences in input RNA using the geometric mean of three reference genes *Aldh1l1, Gapdh* and *Rplp0*. Data preprocessing and analysis was completed using Fluidigm Melting Curve Analysis Software 1.1.0 build 20100514.1234 (Fluidigm) and Real-time PCR Analysis Software 2.1.1 build 20090521.1135 (Fluidigm) to determine valid PCR reactions. Invalid reactions were removed from later analysis. Quantitative RT–PCR was conducted following the MIQE (minimum information for publication of quantitative real-time PCR experiments) guidelines[38]. The array accommodated reactions for 96 samples and 96 genes in total. The pre-amplified cDNA samples from the stimulation experiments were measured together with no reverse transcriptase and no template controls on 96.96 Dynamic Array chips (Fluidigm). Cell-type specific transcripts were also detected for microglia, oligodendrocyte lineage cells and neurons, with any astrocyte samples containing measurable levels of other cell types removed from further analysis. All primer sequences for rat and mouse are listed in Supplementary Tables 1, 2.

Microfluidic qPCR (single-cell samples). Experiments were performed on mice from the transgenic mouse line *Tg(Aldh1l1–eGFP)OFC789Gsat/Mmucd*. For neuroinflammatory injury, P5 mice received a single intraperitoneal injection of either endotoxin-free PBS, or the endotoxin lipopolysaccharide (LPS) from *E. coli* O55:B55 (Sigma–Aldrich) dissolved in normal saline and diluted into endotoxin-free PBS (5 mg kg^{-1}).

For ischaemic injury, published protocols[39] for middle cerebral artery occlusion (MCAO) were modified as follows for P5 mice. Pups were anaesthetized and maintained with 2–3% isoflurane in O_2 on a rectal thermometer feedback heat pad at 37 °C. The head of each mouse was shaved, and cleaned with chlorhexidine, then sterile saline. Mice were injected subcutaneously with antibiotic (25 mg kg^{-1} cefazolin) and analgesic (0.1 mg kg^{-1} buprenorphine). A 4 mm horizontal incision and a 4 mm vertical incision were made to create a skin flap over the temporalis muscle. The temporalis muscle was also incised in a similar manner so that the skull was exposed. A micro drill was used to create a 2 mm diameter hole directly over the middle cerebral artery, the meninges were removed, and the middle cerebral artery was cauterized. The brain surface was rinsed with saline, the temporalis muscle was folded back in to place and the skin was sealed with surgical glue. Mice were placed in a warm cage to recover from anaesthesia until awake and ambulatory. Mice were left for 24 h, at which time mice were killed by decapitation and single-cell suspensions for each control and experimental condition were made for downstream FACS analysis (see below).

For treatment groups, cortices from individual mice were collected separately from four LPS-injected or saline-injected control mice. The hippocampus, cerebellum and olfactory bulbs were removed, as were the meninges. For the MCAO model, the ipsilateral cortex was collected, whereas the contralateral cortex and other brain regions were discarded. Four mice that had undergone MCAO and four sham-operated control surgery mice were used. Dissected tissue was treated as described previously[12]. In brief, dissected tissue was first diced to 1–3 mm and then digested with 200 U of papain enzyme for 90 min at 34 °C in bicarbonate-buffered Earle's balanced salt solution with 0.46% glucose, 26 mM sodium bicarbonate, 0.5 mM EDTA, and 125 U ml^{-1} DNase I (Worthington Biochemicals). Digested tissues were dissociated into single-cell suspensions by gentle trituration, and myelin removed using O4, Mog and GalC supernatants (1:30 at room temperature for 30 min). Myelin and larger tissue clumps were removed by filtering through three layers of Nitex mesh, and cells collected by centrifugation, before resuspension in Dulbecco's PBS (DPBS) containing 0.02% BSA and 125 U ml DNase I and with Live/Dead Fixable Far Red Dead Cell Stain Kit (ThermoFisher, L34973) for fluorescence-activated cell sorting (FACS).

For FACS analysis live astrocytes were isolated at room temperature by FACS at the Stanford Shared FACS Facility on the basis of their GFP expression on a BD Aria II or BD Influx. Cell suspensions were sorted twice sequentially using forward light scatter and SSC to gate single cells, followed by gating for GFP fluorescence in the absence of live/dead stain to select live astrocytes. Individual cells were collected directly into 96-well PCR plates containing RT-STA Mix solution (see below) for microfluidic qPCR. FlowJo software (Treestar) was used to analyse purity of final astrocyte populations.

For single-cell microfluidic qPCR, Fluidigm Advanced Development Protocol 41 for single-cell gene expression using SsoFast Evagreen Supermix with Low ROX was used. Single cells were collect by FACS into a solution containing 5 μl CellsDirect 2× Reaction Mix (Thermo Scientific, 11753100), 1.0 μl Superscript III RT Platinum Taq Mix, 2.0 μl 10× primer mix (as for other microfluidic assays, primers at 500 nM), and 2.0 μl nuclease-free water, and frozen at −20 °C until processed.

For microfluidic qPCR, cells were defrosted on ice and pre-amplification PCR completed using the following thermocycling protocol: 50 °C for 15 min, 95 °C for 2 min, 18 cycles of 95 °C for 15 s and 60 °C for 4 min, hold at 4 °C. Excess primers were removed with 3.6 μl of Exonuclease I from *E. Coli* according to the manufacturer's protocol (New England BioLabs, M0293S): 37 °C for 30 min, 80 °C for 15 min, hold at 4 °C. This final pre-amplified sample was diluted fivefold in TE Buffer (TEKnova, T0224). Five microlitres of diluted sample were loaded into each sample inlet of a 96.96 Dynamic Array chip (Fluidigm Corporation, San Francisco, CA, USA) and 5 μl from an assay mix containing DNA-assay loading reagent as well as forward and reverse primers (10 pmol μl^{-1}), was loaded into each detector inlet. The chip was then placed in the NanoFlexTM 4-IFC Controller (Fluidigm) for loading and mixing. After loading, the chip was processed in the BioMarkTM Real-Time PCR System (Fluidigm) using a cycling program of 10 min at 95 °C followed

by 40 cycles of 95 °C for 15 s and 60 °C for 30 s and 72 °C for 30 s. After completion of qPCR, a melting curve of amplified products was determined. Data were collected using BioMarkTM Data Collection Software 2.1.1 build 20090519.0926 (Fluidigm) as the cycle of quantification (C_q), where the fluorescence signal of amplified DNA intersected with background noise. Data preprocessing and analysis was completed using Fluidigm Melting Curve Analysis Software 1.1.0 build 20100514.1234 (Fluidigm) and Real-time PCR Analysis Software 2.1.1 build 20090521.1135 (Fluidigm) to determine valid PCR reactions. Invalid reactions were removed from later analysis. Data were analysed following published protocols for single-cell RT–qPCR[40].

Standard qRT–PCR. Total RNA was extracted and cDNA synthesized as above. Quantitative RT–PCR was run using 2 μl cDNA and SYBR green chemistry (Applied Biosystems/ThermoFisher Scientific, 4334973) using the supplier's protocol and a cycling program of 2 min at 95 °C followed by 40 cycles of 95 °C for 3 s and 60 °C for 30 s on a Mastercycler Epgradient S (Eppendorf). After completion of qPCR, a melting curve of amplified products was determined. Data were collected using an Eppendorf Mastercycler Ep Realplex v2.2 (Eppendorf). Primer sequences for rat and mouse are listed in Supplementary Tables 1, 2. Primer sequences for human as follows: *hALDH1L1* (forward, AGGGGCTGTTTTTCTCTCGG; reverse, CATGGTAGCAGGAGGGTTGG), *hC3* (for AD, HD, PD, ALS: forward, AAAAGGGGCGCAACAAGTTC; reverse, GATGCCTTCCGGGTTCTCAA; for MS: forward, CCCTGGCTCCACAGTTCTCT; reverse, CAAGGAGTCCTGCTTGACCG), *hRPLP0* (forward, GAAACTCTGCATTCTCGCTTCC; reverse, GATGCAACAGTTGGGTAGCCA), *hS100A10* (forward, CACGTACTAAGGAAGGCGCA; reverse, TGTGGTCCGTTGAAGCCTTG).

Western blot. Protein samples (conditioned growth medium) were collected at 4 °C in PBS buffer containing Complete Protease Inhibitor Cocktail (Roche) and concentrated with Amicon Ultra-15 centrifugal filter units, with a 30-kDa size exclusion (EMD Millipore). The total protein concentration of samples was determined by Bradford assay (Sigma) and equal amounts of total protein were loaded onto 12% Tris–HCl gels (Bio-Rad). Following electrophoresis (100 V for 45 min), proteins were transferred to Immobilon-P membranes (EMD Millipore). Blots were probed overnight at 4 °C with 1:200 rabbit anti-glypican2 (Abcam, ab129526), 1:200 rabbit anti-versican (Abcam ab19345), 1:1,000 rabbit anti-syndecan1 (Invitrogen, 36-2900), 1:1,000 rabbit anti-brevican (MyBioSource, MBS710876), 1:1,000 mouse anti-neurocan (EMD Millipore, MAB5234), 1:200 mouse anti-NG2 (abcam, ab50009), 1:50 goat anti-mouse C1q (Santa Cruz Biotechnology, sc-365301). Blots were incubated with HRP-conjugated secondary antibodies at 1:5,000 for 2 h at room temperature and developed using ECL Prime Western Blotting Detection Reagent (GE Healthcare). Visualization and imaging of blots was performed with a FluorochemQ System (ProteinSimple).

Cytokine array screen. Conditioned medium from immunopanned purified and cultured microglia grown in non-reactive, or LPS-induced reactive state was collected as above and 100 μg of total protein was incubated with a Rat Cytokine Antibody Array Kit (R&D Systems, ARY008) according to the manufacturer's protocols.

Immunohistochemistry (rodent). Animals (rats or mice) were anaesthetized with a ketamine (100 mg kg^{-1})/xylazine (20 mg kg^{-1}) cocktail, and perfused with ice-cold PBS followed by ice-cold 4% paraformaldehyde at approximately 70% cardiac output. Dissected brains were post-fixed overnight in 4% paraformaldehyde at 4 °C, and cryoprotected in 30% sucrose. For retinal immunohistochemistry, whole eyeballs were dissected and placed in ice-cold 4% paraformaldehyde for 10 min, and then washed in DPBS before dissecting the retina away from the rest of the eyeball and post-fixing in 4% paraformaldehyde overnight a 4 °C. Both brains and whole retinas were embedded in OCT compound (Tissue-Tek) and 10 μm tissue sections were prepared with a Leica cryostat. The following antibodies were used: 1:5,000 rabbit anti-GFAP (DAKO, Z0334), 1:500 rat anti-GFAP (Invitrogen, clone 2.2B10), rabbit anti-AQP4 (Sigma, HPA014784), 1:500 rabbit anti-RBPMS (PhosphoSolutions, 1830-RBPMS), 1:500 mouse anti-CD68 (AbD Serotec, clone 514H12), 1:500–1,500 rabbit anti-hC3D (DAKO, A0063). Primary antibodies were visualized with appropriate secondary antibodies conjugated with Alexa fluorophores (Invitrogen).

Immunohistochemistry (human). All human brain tissue samples were obtained with appropriate consent given before collection of tissue. Tissue samples were obtained from the following tissue banks: the Stanford Alzheimer's Disease Research Centre (AG047366), the Stanford Health Care Brain Bank, the University of Pennsylvania Institute on Aging, The Arizona Aging & Disability Resource Centres (AG019610) and Banner Sun Health for Alzheimer's brain samples; the UK Multiple Sclerosis Tissue Bank, funded by the Multiple Sclerosis Society of Great Britain and Northern Ireland (registered charity 207495) for multiple sclerosis tissue samples; the Department of Pathology, Johns Hopkins University School of Medicine for Parkinson's disease samples; the Neurological Foundation of New Zealand Human Brain Bank at the University of Auckland and the Boston University Medical Centre for Huntington's disease; and the University of Pennsylvania Institute on Aging for amyotrophic lateral sclerosis patient samples.

Immunohistochemistry of human post-mortem MS tissue (see Supplementary Table 3) was carried out on 20-μm thick snap-frozen sections, fixed with ice-cold methanol. Blocking steps included peroxidase blocking with H_2O_2, avidin and biotin blocking (Vector), and normal serum blocking with 10% serum of species in which secondary antibodies were raised, diluted in 1× PBS with 0.01% Triton X (PBST). Incubations with primary antibodies diluted in PBST were overnight at 4 °C (mouse anti-rat MOG, Millipore, MAB5680, 1:1,000; MHC-II, Abcam HLA DR, ab80658, 1:50; mouse anti-human CD68, AbD Serotec, MCA1815, 1:200; rat anti-GFAP, Invitrogen, MA5-12023, 1:500; mouse anti-human S100A10, Invitrogen, MA5-15326, 1:1,000; rabbit anti-human C3D, DAKO, A0063, 1:1,000), and detection was achieved by signal amplification using biotinylated secondary antisera (Vector) followed by avidin–peroxidase (Vectastain ABC, Vector). Diaminobenzidine (DAKO) was used as chromogenic substrate. Negative control sections without primary antibodies were processed in parallel. Sections were counterstained with either haematoxylin, or 4′,6-diamidino-2-phenylindole (DAPI). Double- and triple-fluorescence staining was performed with fluorochromes tagged to streptavidin and secondary antibodies (Alexa Fluor 488, 594 and 647, Invitrogen).

Immunofluorescence double labelling for GFAP and C3 of human post-mortem AD tissue (see Supplementary Table 4) and PD tissue (see Supplementary Table 5) was carried out on 16-μm-thick snap-frozen sections, fixed with ice-cold 1:1 methanol:acetone for 5 min at room temperature. Endogenous protein activity was blocked with 10% serum of species in which secondary antibodies were raised, diluted in 1× PBST for 2 h at room temperature. Primary antibody incubations were carried out overnight at 4 °C; for AD, rat anti-mouse GFAP (1:1,000, Sigma, G3893) and for PD, mouse anti-porcine GFAP (1:1,000, Millipore, MAB360) and rabbit anti-human C3D (1:1,000, DAKO, A0063). Detection was achieved with appropriate Alexa fluorescent secondaries for 3 h at room temperature (diluted 1:5,000 in PBST, Invitrogen).

Fluorescence *in situ* hybridization of human post-mortem tissue. Immunofluorescence double labelling for S100β and fluorescent *in situ* hybridization (FISH) for *C3* was carried out on 10-μm-thick frozen sections of human tissue fixed with 4% paraformaldehyde and cryopreserved in 30% sucrose (see tissue sample details in Supplementary Tables 4, 6, 7). To generate the *C3* antisense RNA probe, *C3* was synthesized from the pCMV SPORT6 C3 plasmid (Open Biosystems reference MHS6278-202800305), digested with SalI and RNA was transcribed from the T7 promoter. Dioxigenin labelling was carried out using an RNA labelling kit (Roche) before performing alkaline hydrolysis at 60 °C for 16 min. A sense probe was also generated from the same plasmid but in this case digestion was carried out with XhoI and RNA transcribed form the SP6 promoter. For FISH, tissue sections were incubated with RNA probes overnight at 64 °C, and binding was then detected with anti-digoxigenin antibodies (Roche). Staining was amplified using a TSA staining Kit (Perkin Elmer). Immunostaining for S100β (1:1,000, DAKO, Z0311) was subsequently performed as described above for IHC with GFAP and C3.

Synapse formation assay. We purified retinal ganglion cells from P5 rats by sequential immunopanning to greater than 99% purity and cultured them in serum-free medium as previously described[41]. Control and A1 astrocytes were plated on inserts and co-cultured with RGCs for 5–10 days. For quantification of structural synapses, RGCs were fixed and stained with antibodies against the presynaptic marker bassoon and postsynaptic marker homer. Synapse number and size were quantified by a custom-written Matlab program[14].

Survival/cell toxicity assay. Control or A1 astrocytes (see above) were grown for 7 days in serum-free medium supplemented with 5 ng ml^{-4} HBEGF[18]. Cells were then treated with Il-1α, TNF and C1q or an equivalent volume of 1× DPBS and cells left for an additional 24 h. At this time, conditioned medium was collected with cOmplete, Mini, EDTA-free Protease Inhibitor Cocktail (Sigma/Roche, 04693159001) and concentrated at 30 kDa with Amicon Ultra-15 Centrifugal Filter Units (Millipore, UFC903024) until approximately 30–50× concentrated. A Bradford assay was performed to determine total protein concentration, and 1–50 μg ml^{-1} total protein was added to purified cell cultures of neurons, oligodendrocytes, oligodendrocyte precursor cells (OPCs), endothelial cells, astrocytes, pericytes or microglia (plated at 1,000 cells per well in poly-D-lysine-coated 96-well plates, grown for 5 days in serum-free base medium) and viability assed using the Live/Dead Kits for mammalian cells (Thermo Fisher Scientific, L3224). Additional experiments were done on RGCs and oligodendrocytes using heat-inactivated A1-astrocyte-conditioned medium (ACM, 20 min treatment at 60 °C) or protease treatment of A1 ACM (0.01 U ml^{-1} plasmin from human plasma, Sigma, P1867), 2 h at room temperature. Protease treatment was halted with phenylmethylsulfonyl fluoride (Sigma, 78830) and aprotinin (Sigma, A4529), at final concentrations of 2 mM and 0.55 TIU ml^{-1}, respectively. Equivalent amounts of astrocyte base medium proteins (BSA, transferrin, HBEGF and so on) were added back

to protease-treated A1 ACM before treating cells). Viability was again assessed at 24 h as before. At least six independent experiments were conducted for each condition. For each experiment, four non-overlapping 20× fields per well were quantified in six wells.

Motor neuron subtype toxicity assays. Motor neurons were purified from embryonic day 15 rats using immunopanning (192 hybridoma clone)[35], plated at 1,000 cells per well in poly-D-lysine-coated 96-well plates and grown for 5 days in serum-free base medium. At this time cells were treated with A1 ACM (50 μg ml^{-1} total protein) and cells left until maximum death was seen (approximately 72–120 h), as determined by Live/Dead kit for mammalian cells (Thermo Fisher Scientific, L3224). Total RNA from remaining (resistant) cells was extracted using the RNeasy Plus kit (Qiagen) and cDNA synthesis performed using the SuperScript VILO cDNA Synthesis Kit (Invitrogen) according to supplier protocols, and RT–PCR for motor neuron subtype specific transcripts completed: all motor neurons, *Ngfr* (forward, CTGCTGCTGATTCTAGGGATGT; reverse, ATCTGCACACTGCATCGTCT), *FoxP1* (forward, CAACGTGCCCAT TTCTTCAGC; reverse, AGATTCAAGAATGGCCTGCCT); pre-ganglionic motor neurons, *Ne2f2* (forward, AAGCACTACGGCCAGTTCAC; reverse, CCTCTGTACAGCTTCCCGTC); alpha motor neurons, *Rbfox* (forward, CTTGTCCGTTTGCTTCCAGG; reverse, GGAAGGTTTCACATGGTTCCG); gamma motor neurons, *Wnt7a* (forward, CGGACGCCATCATCGTCATA; reverse, CTCCCGACTCCCCACTTTGA), *Esrrg* (forward, TTGAACCCGAGACTCTC CCA; reverse, GCAGAGAAGCCTTTCCGACT).

Bacteria cultures and killing assays. Bacterial strains include *Salmonella typhimurium* (SL1344), *Burkholderia thailandensis* (E264), and *Shigella flexneri* (M90T). *S. typhimurium* was grown in LB broth (BD Biosciences). *B. thailandensis* and *S. flexneri* were grown in tryptic soy broth (TSB; BD Biosciences). All strains were grown in 2 ml broth overnight from a frozen stock with aeration at 37 °C. Bacteria were subcultured 1:1,000 into broth (*S. typhimurim* and *S. flexneri* into MGM–MES medium[42] and *B. thailandensis* into TSB) and 50% supernatant from control astrocytes or A1 reactive astrocytes at serial dilutions from 0–100 μg ml^{-1}. At 16 h of growth the OD_{600} was recorded.

Differentiation of human embryonic stem cells to dopaminergic neurons. H1 human embryonic stem cells (ES cells, Wi Cell) were cultured using standard protocols on inactivated mouse embryonic fibroblasts. Differentiation of hES cells to dopamine neurons was done as described previously[43]. Human ES cells were cultured on matrigel (Corning, CB-40234)-coated plates at a density of 40,000 cells per cm^2 in SRM medium containing growth factors and small molecules, including FGF8a (100 ng ml^{-1}, R&D Systems, 423-F8-025/CF), SHH C25II (100 ng ml^{-1}, R&D Systems, 464-SH-025/CF), LDN193189 (100 nM, Stemgent Inc., 04-0074-02), SB431542 (10 μM, Stemgent Inc., 04-0010), CHIR99021 (3 μM, Stemgent Inc., 04-0004-02) and Purmorphine (2 μM, Stemgent Inc., 04-0009) for the first five days. For the next six days, cells were maintained in neurobasal medium containing B27 without vitamin A (Life Technologies, 12587-010), N2 supplement (Life Technologies, 17502048) along with LDN193189 and CHIR99021. In the final stage, cultures were lifted and replated at a density of 400,000 cells per cm^2 on polyornithine- and laminin-coated plates in a neurobasal medium containing B27 without vitamin A, containing BDNF (20 ng ml^{-1}, R&D Systems, 248-BD-025/CF), GDNF (20 ng ml^{-1}, R&D Systems, 212-GD-010/CF), TGFβ (1 ng ml^{-1}, R&D Systems, 243-B3-002/CF) ascorbic acid (0.2 mM, Sigma, A4034), cAMP (0.5 mM, Sigma D0627) and DAPT (10 μM, Stemgent, 04-0041) until maturation. Once mature (after approximately 60 days), toxicity assays with A1 ACM were performed as outlined above.

TUNEL staining of apoptotic cells in mouse hippocampus. Neuronal cell death was detected *in vivo* in wild-type and single-knockout animals (*Il1a*$^{-/-}$, *TNF*$^{-/-}$ or *C1qa*$^{-/-}$) using TUNEL staining of 12-μm 4%-paraformaldehyde-fixed, frozen sections of hippocampus using the *in situ* cell death detection kit, TMR red (Roche, 12156792910) using the supplier's protocol.

Depletion of microglia using pexidartinib. Pexidartinib (PLX-3397, SelleckChem, S7818), a CSF1R inhibitor, was administered *ad libitum* to P21 wild-type C57Bl/6 mice at 290 mg kg^{-1} in AIN-76A Rodent Diet (Research Diets Inc., D10001) for 7 days to eliminate microglia[44]. At this stage flow cytometry showed around a 95% decrease in microglia cell number (Extended Data Fig. 1). These microglia-depleted animals were used for optic nerve crush (see below) and neuroinflammatory experiments (with intraperitoneal (i.p.) injection of 5 mg kg^{-1} LPS).

Flow cytometry analysis of *Csf1r*$^{-/-}$ and PLX-3397-treated animals. Both *Csf1r*$^{-/-}$ and PLX-3397-treated animals (and appropriate controls, *Csf1r*$^{+/+}$ and control chow-treated animals, respectively) received an i.p. injection of LPS (5 mg kg^{-1}). Twenty-four hours after LPS injection, animals were killed and brains prepared for downstream processing (see below).

For P28 PLX-3397-treated animals, brain cell dissociation and staining was performed as described previously[15] with minor changes, specifically the addition of cold PBS intravascular perfusion, dissection of the cortex rather than whole brain, and the use of a different fluorophore panel. In brief, cortices from PLX-3397 and control treatments were dissected from anaesthetized, cold PBS-perfused mice at P28. Cortices were homogenized in ice-cold HBSS supplemented with 15 mM HEPES and 0.5% glucose by five gentle strokes in a 7-ml glass dounce homogenizer. Dissociated cell suspensions were run through MACS myelin depletion columns, stained with a dead cell marker (Live/Dead, Life Technologies, L23101), and then immunostained using antibodies specific to TMEM119 (custom antibody[15], secondary antibody Biolegend 406410), CD45 (eBioscience 25-0451-82) and CD11b (Biolegend 101228). Samples were analysed on an LSR II (Becton Dickinson), and data were processed using FlowJo software (Treestar). Data were collected on an instrument in the Stanford Shared FACS Facility obtained using the NIH S10 Shared instrument Grant (S10RR027431-01). Debris, doublets, and dead cells were excluded using FSC/SSC, FSC-H/FSC-W, and green fluorescence gates, respectively.

For P8 *Csf1r*$^{-/-}$ animals, brains were processed identically except that the myelin depletion step was removed and cells were passed through a fine nylon mesh to filter debris (Tetko HC3-20).

Retro-orbital nerve crushes. P14 Sprague Dawley rats or P21–P28 mice were anaesthetized with 2.5% inhaled isoflurane in 2.0 l O_2 per min. Without incision to the orbital rim, the supero-external orbital contents were blunt-dissected, the superior and lateral rectis muscles teased apart, and the left optic nerve exposed. The nerve was crushed for 3–5 s at approximately 2 mm distal to the lamina cribrosa. After surgery, the eye fundi were checked to ensure retinal blood flow was intact. Some rats also received a 2 μl intravitreal injection of neutralizing antibodies to Il-1α (150 μg μl^{-1}, Abcam, ab9614), TNF (150 μg μl^{-1}, Cell Signaling Technology, 7321), and C1q (Quidel, A301), rabbit IgG control (150 μg μl^{-1}, Abcam, ab27472), or PBS at day 0 (the time of optic nerve crush, for 7 and 14 day experiments) or day 7 (for some 14 day experiments). Retinas were collected for qPCR analysis and immunofluorescence analysis at 7 and 14 days.

Synaptosome/myelin purification and *in vitro* engulfment assay. Synaptosomes[45] and crude CNS myelin[46] were purified as described previously, and conjugated with pHrodo Red, succinimidyl ester (Thermo Fisher Scientific, P36600) in 0.1 M sodium carbonate (pH 9.0) at room temperature with gentle agitation. After a 2-h incubation, unbounded pHrodo was washed out by multiple rounds of centrifugation and pHrodo-conjugated synaptosomes/myelin were re-suspended with isotonic buffer containing 5% DMSO for subsequent freezing. Purified control and A1 astrocytes from P6 rat pups (see above) were incubated with 5 μl pHrodo-conjugated synaptosomes for 24 h, or 800 μg ml^{-1} medium pHrodo-conjugated myelin debris and imaged at 1 h intervals. Live astrocytes were imaged with an epifluorescence time lapse microscope (IncuCyte Zoom System) to analyse engulfed pHrodo-conjugated particles. For image processing analysis, we took 9 images per well using a 20× objective lens from random areas of the 24-well plates and calculated the phagocytic index by measuring the area of engulfed synaptosomes/myelin (fluorescent signal) normalized to the area of astrocytes, using ImageJ. Relative engulfment ability was calculated by normalizing the phagocytic index of control (non-reactive) astrocytes to A1 astrocytes[3].

***In vivo* synapse engulfment assay.** *Tg(Aldh1l1–eGFP)OFC789Gsat/Mmucd* transgenic mice were used to visualize astrocytes in all *in vivo* engulfment assays. Pups were anaesthetized with isoflurane and 5 mg kg^{-1} LPS was injected i.p. at P3. Twenty hours later 1 μl of cholera toxin-β subunit (CTB) conjugated with Alexa594 (Invitrogen, 1 mg ml^{-1} in normal saline) was injected into the contralateral eye. After 24 h mice were killed and half had the dorsal lateral geniculate nucleus (dLGN) dissected out for microfluidic qPCR analysis, while the remainder were perfused with PBS followed by 4% paraformaldehyde at 70% cardiac output and brains were dissected, post-fixed overnight at 4 °C and transferred to 15% and 30% sucrose for 24 h each at 4 °C. Brains were sectioned at 50 μm and floating coronal sections containing the dLGN were mounted on glass slides and used for analysis of the dLGN. For each dLGN, two fields (the tip and medial portions of dLGN that contain both contra- and ipsilateral projections) were imaged using a Zeiss LSM510 inverted confocal microscopy to obtain 50–70 consecutive optical sections with 0.3-μm interval thickness. ImageJ was used to remove outliers (radius 2.0 pixels and threshold 20) from all channels and to subtract background from CTB images (rolling bar radius 50 pixels). An image-processing algorithm (Matlab, Mathworks) was used to localize CTB-labelled RGC projections engulfed by astrocytes by subtracting CTB-labelled projections outside of the Aldh1l1–eGFP positive cells. The phagocytic index was calculated by measuring the total volume of engulfed CTB-labelled RGC projections normalized to the total volume of astrocytes in a given *z* stack. Relative engulfment ability was calculated by normalizing the phagocytic index of experimental groups to the control group[3].

Electrophysiology. Whole-cell patch-clamp recordings from cultured RGC neurons were performed at room temperature in an isotonic saline solution (in mM: NaCl 125, $NaHCO_3$ 25, KCl 2.5, NaH_2PO_4 1.25, glucose 25, $MgCl_2$ 1, $CaCl_2$ 2).

Patch electrodes with resistances of 2.5–3.5 MΩ were pulled from thick-walled borosilicate glass capillaries and were filled with an internal solution containing (in mM) potassium gluconate 130, NaCl 4, EGTA 5, $CaCl_2$ 0.5, HEPES 10, MgATP 4, Na_2GTP 0.5 (pH 7.2 with KOH). Miniature excitatory postsynaptic currents (mEPSCs) were recorded in TTX (1 μM, Alomone) from a holding potential of −70 mV. Series resistance was monitored throughout the recording and was <20 MΩ. Data were sampled at 50 kHz and filtered at 1 kHz using pClamp 9.2, and offline analysis of mEPSCs was performed using Clampfit 10.3 (Molecular Devices).

Proliferation, differentiation and motility assays. Cultures of OPCs were prepared by immunopanning and grown as outlined in Methods. To measure proliferation, OPCs were grown for 24 h in OPC proliferation medium[47] and then changed into OPC medium containing 10 μM EdU (ThermoFisher, C10339) and varying concentrations of A1 or resting ACM (0–50 μg ml^{-1} total protein). After 5 days, the cells were fixed, permeabilized, and stained for EdU and DNA (Hoechst 33342) according to the protocol for the Click-It Edu Imaging Kit. To measure differentiations of OPCs into mature oligodendrocytes, 1 μg ml^{-1} A1 ACM was added to OPC cultures and they were imaged at 24 h intervals with a phase time lapse microscope (IncuCyte Zoom System). Images were analysed and number of primary processes extending from the cell soma were counted. A cell was considered an OPC with 0–2 processes, a differentiating oligodendrocyte with 4–5 processes, and a mature oligodendrocyte with >5 primary processes. Before differentiation into mature oligodendrocytes, OPC migration was measured using the Template Matching and Slice Alignment and MTrackJ plugins for ImageJ. Astrocyte motility was measured using the same ImageJ plugin, with cells grown at a density of 5,000 cells per cm^2 in HBEGF-containing astrocyte growth medium.

Statistical analysis and power calculations. All statistical analyses were done using GraphPad Prism 7.00 software. Most data were analysed by one-way ANOVA followed by Dunnett's multiple post hoc test for comparing more than three samples, and two-sample unpaired *t*-tests for comparing two samples with 95% confidence. Two-sample Kolmogorov–Smirnov tests with 95% confidence were used for electrophysiology experiments in Fig. 2g. Power calculations were performed using G*Power Software V 3.1.9.2 (ref. 48). Group sizes were used to provide at least 80% calculable power with the following parameters: probability of type I error (0.05), conservative effect size (0.25). Four to eight treatment groups with multiple measurements were obtained per replicate.

Data availability. The data that support the findings of this study are available from the corresponding author upon reasonable request.

34. Stephan, A. H. *et al.* A dramatic increase of C1q protein in the CNS during normal aging. *J. Neurosci.* **33,** 13460–13474 (2013).
35. Graber, D. J. & Harris, B. T. Purification and culture of spinal motor neurons from rat embryos. *Cold Spring Harb. Protoc.* **4,** 319–326 (2013).
36. Zhou, L., Sohet, F. & Daneman, R. Purification of endothelial cells from rodent brain by immunopanning. *Cold Spring Harb. Protoc.* **1,** 65–77 (2014).
37. Zhou, L., Sohet, F. & Daneman, R. Purification of pericytes from rodent optic nerve by immunopanning. *Cold Spring Harb. Protoc.* **6,** 608–617 (2014).
38. Bustin, S. A. *et al.* The MIQE guidelines: minimum information for publication of quantitative real-time PCR experiments. *Clin. Chem.* **55,** 611–622 (2009).
39. Doyle, K. P. & Buckwalter, M. S. A mouse model of permanent focal ischemia: distal middle cerebral artery occlusion. *Methods Mol. Biol.* **1135,** 103–110 (2014).
40. Ståhlberg, A., Rusnakova, V., Forootan, A., Anderova, M. & Kubista, M. RT-qPCR work-flow for single-cell data analysis. *Methods* **59,** 80–88 (2013).
41. Winzeler, A. & Wang, J. T. Purification and culture of retinal ganglion cells from rodents. *Cold Spring Harb. Protoc.* **7,** 643–652 (2013).
42. Yu, X.-J. J., Liu, M. & Holden, D. W. SsaM and SpiC interact and regulate secretion of *Salmonella* pathogenicity island 2 type III secretion system effectors and translocators. *Mol. Microbiol.* **54,** 604–619 (2004).
43. Kriks, S. *et al.* Dopamine neurons derived from human ES cells efficiently engraft in animal models of Parkinson's disease. *Nature* **480,** 547–551 (2011).
44. Elmore, M. R., Lee, R. J., West, B. L. & Green, K. N. Characterizing newly repopulated microglia in the adult mouse: impacts on animal behavior, cell morphology, and neuroinflammation. *PLoS One* **10,** e0122912 (2015).
45. Dunkley, P. R., Jarvie, P. E. & Robinson, P. J. A rapid Percoll gradient procedure for preparation of synaptosomes. *Nat. Protocols* **3,** 1718–1728 (2008).
46. Larocca, J. N. & Norton, W. T. Isolation of Myelin. *Curr. Protoc. Cell Biol.* Ch, 3, Unit3.25 (2007).
47. Zuchero, J. B. *et al.* CNS myelin wrapping is driven by actin disassembly. *Dev. Cell* **34,** 152–167 (2015).
48. Faul, F., Erdfelder, E., Lang, A.-G. G. & Buchner, A. G*Power 3: a flexible statistical power analysis program for the social, behavioral, and biomedical sciences. *Behav. Res. Methods* **39,** 175–191 (2007).

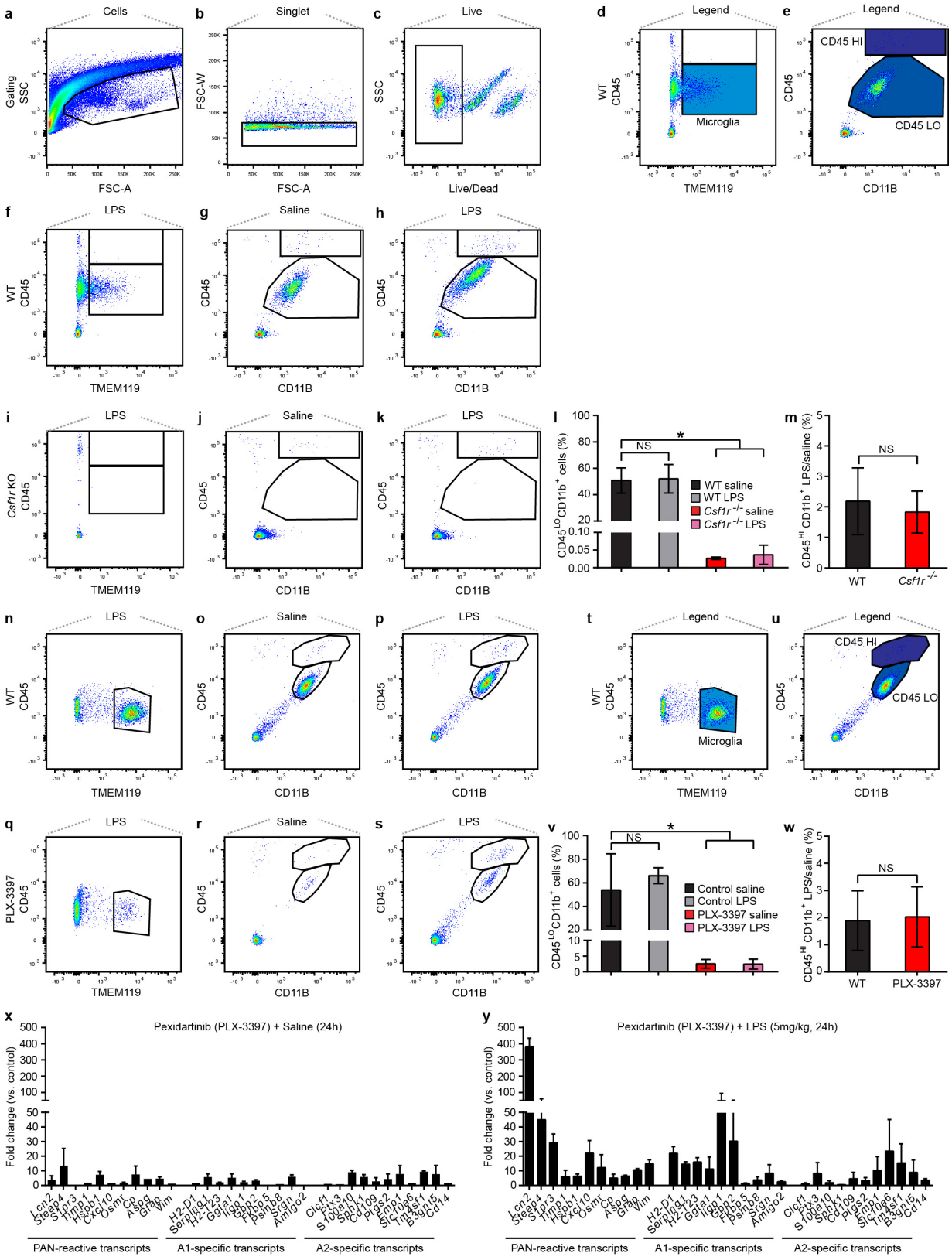

Extended Data Figure 1 | See next page for caption.

Extended Data Figure 1 | *Csf1r*$^{-/-}$ mice lack microglia and have no compensatory increase in brain myeloid cell populations after LPS or vehicle control injections. a–c, Gating strategy (live, single cells) for subsequent analysis of surface protein immunostaining. **d, e**, Gating strategy for TMEM119^{+} (microglia) and CD45^{low}CD11b^{+} cells used for further analysis. **f–h**, Representative plots showing abundant macrophage populations in P8 wild-type mice: CD45^{low}TMEM119^{+}/TMEM119^{-}, and CD45^{high} brain macrophages (**f**), CD11B^{+}CD45^{low} and CD11B^{+}CD45^{high} cells after saline (**g**) or LPS (**h**) injection. **i–k**, Representative plots showing near-complete absence of brain macrophages in *Csf1r*$^{-/-}$ mice: CD45^{low}TMEM119^{-}TMEM119^{-}, and CD45^{high} brain macrophages (**i**), CD11B^{+}CD45^{low} and CD11B^{+}CD45^{high} cells after saline (**j**) and LPS (**k**) injection. **l**, Relative abundance of CD11B^{+}CD45^{low} macrophages after LPS or control injection in wild-type compared to *Csf1r*$^{-/-}$ mice, expressed as percentage of total gated events shown in **a**. **m**, Relative abundance of CD11B^{+}CD45^{high} cells after LPS treatment, normalized to saline control injection in wild-type and *Csf1r*$^{-/-}$ animals. **n–p**, Pexidartinib (PLX-3397)-treated adult mice have a pronounced reduction in the number of microglia and no increase in myeloid cell infiltration after LPS-treatment compared to vehicle control treatment. Representative plots showing abundant macrophage populations in P28 wild-type control mice: TMEM119^{+} microglia (**n**), CD11B^{+}CD45^{low} and CD11B^{+}CD45^{high} cells after saline (**o**) and LPS (**p**) injection. **q–s**, Representative plots showing a large reduction in macrophage populations after PLX-3397 treatment: TMEM119^{-} microglia (**q**), CD11B^{+}CD45^{low} and CD11B^{+}CD45^{high} cells after saline (**r**) and LPS (**s**) injection. **t**, **u**, gating strategy for TMEM119^{+} (microglia) and CD45^{low}CD11b^{+} cells used for analysis. **v**, Relative abundance of CD11B^{+}CD45^{low} macrophages in wild-type compared to PLX-3397-treated mice, expressed as percentage of total gated events. **w**, Relative abundance of CD11B^{+}CD45^{high} cells after LPS treatment, normalized to saline control injection in wild-type and PLX-3397-treated animals. **x, y**, Fold change data from microfluidic qPCR analysis of wild-type and PLX-3397-treated mouse immunopanned astrocytes collected 24 h after i.p. injection with saline or LPS (5 mg kg^{-1}). We found that we could only deplete approximately 95% of microglia using this drug (**v**), and it is probable that the remaining 5% that are sufficient to induce this strong level of A1 reactivity in astrocytes following LPS-induced neuroinflammation, also account for the death of retinal ganglion cells in optic nerve crush experiments (Figs 1e, 4l). $n = 3$–6 individual animals per treatment condition and genotype. Data are mean ± s.e.m. $^{*}P < 0.05$, one-way ANOVA (**l**, **v**); $P = 0.77$ (**m**), $P = 0.90$ (**w**), Student's *t*-test, compared to age-matched wild-type control.

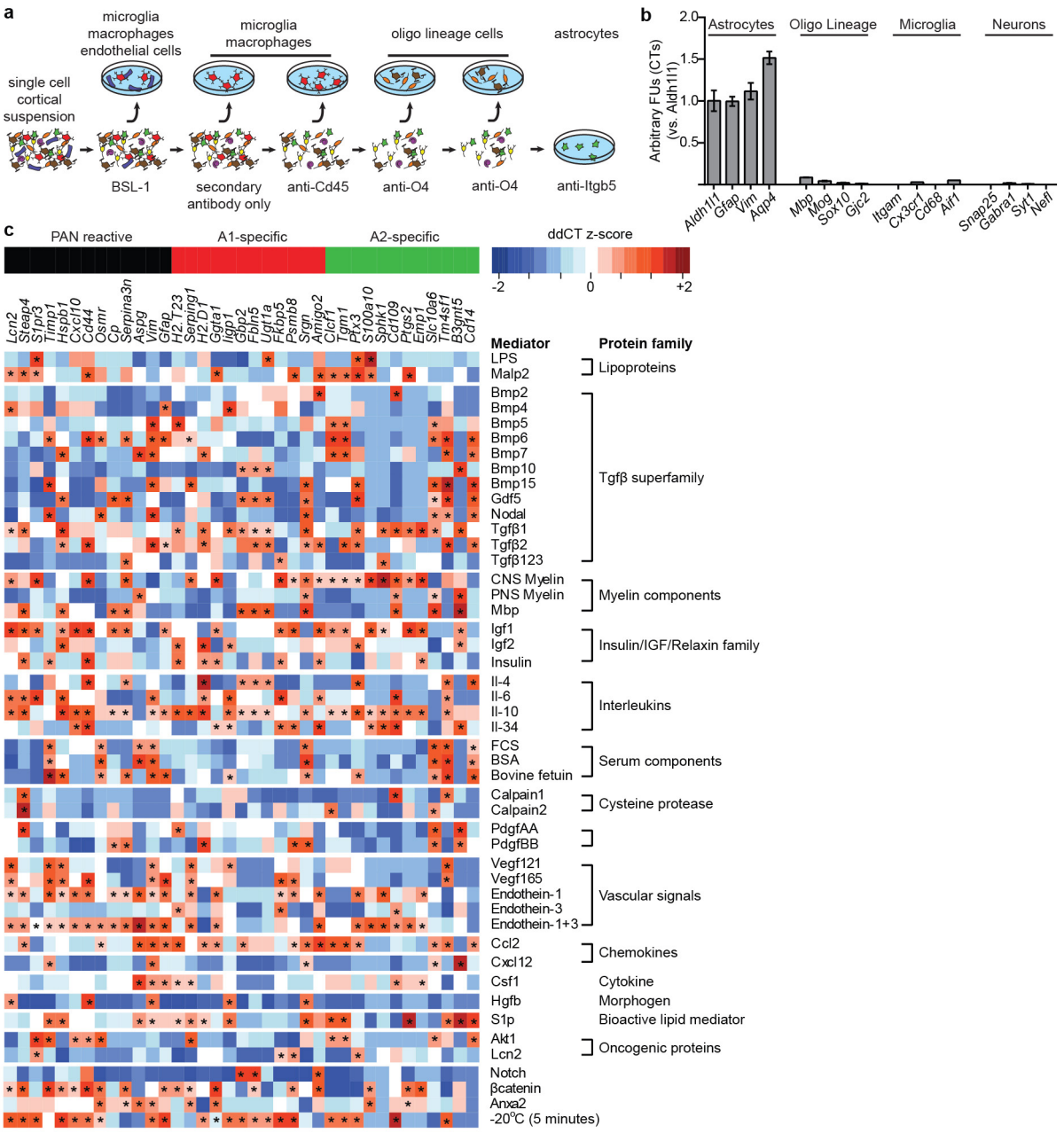

Extended Data Figure 2 | Screen for A1 mediators. a, Immunopanning schematic for purification of astrocytes. These astrocytes retain their non-activated *in vivo* gene profiles. **b**, Purified cells were >99% pure with very little contamination from other central nervous system cells, as measured by qPCR for cell-type specific transcripts. **c**, Heat map of pan-reactive and A1- and A2-specific reactive transcript induction following treatment with a wide range of possible reactivity inducers. These factors did not produce an A1-astrocyte phenotype alone or in combination. $n = 8$ per experiment. $^*P < 0.05$, one-way ANOVA (increase compared to non-reactive astrocytes).

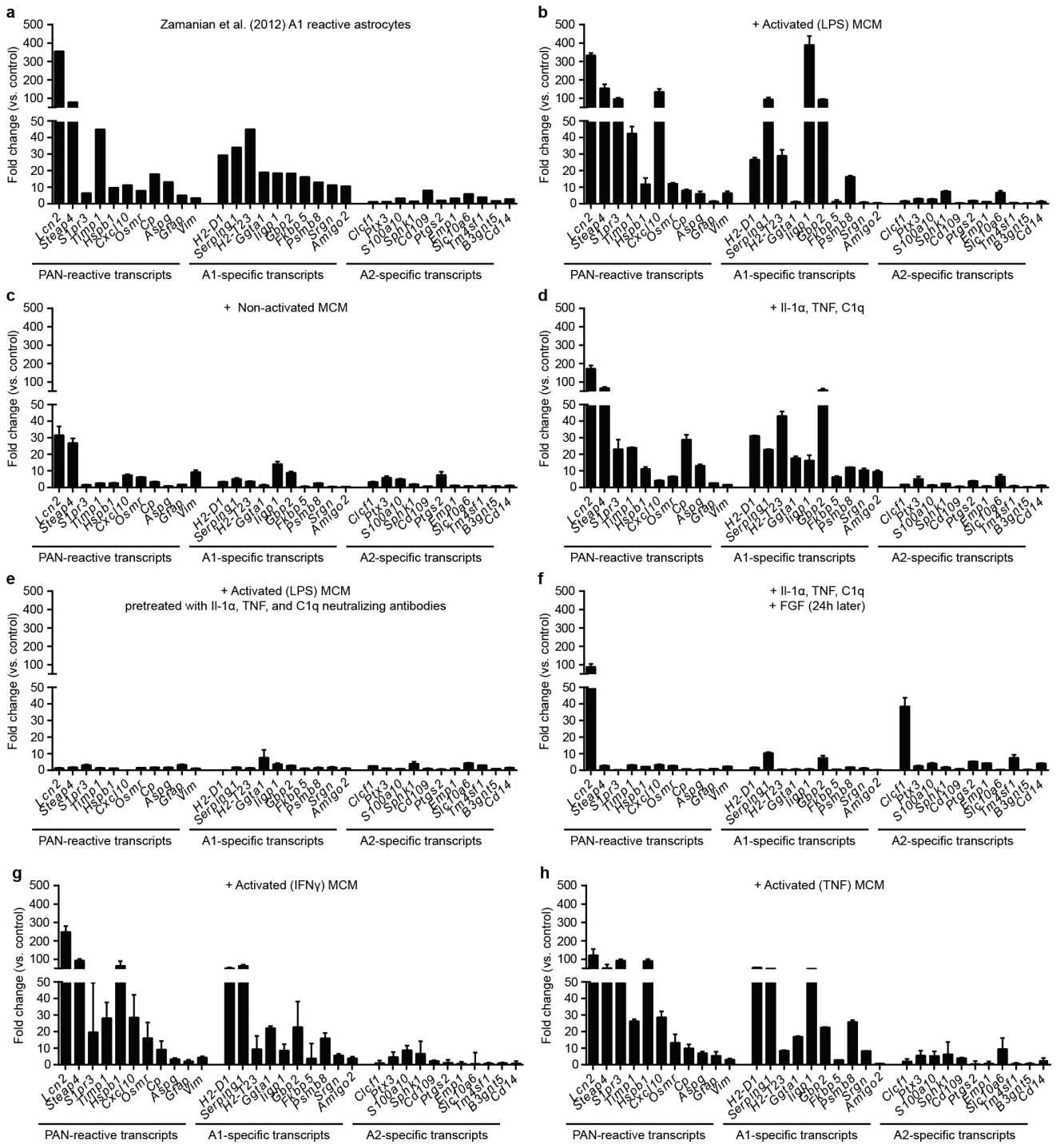

Extended Data Figure 3 | Screen for A1 mediators. a, Fold change data from published microarray datasets of A1 (neuroinflammatory) reactive astrocytes. **b–h**, Microfluidic qPCR analysis of purified astrocytes treated with lipopolysaccharide (LPS)-activated microglia conditioned medium (**b**), non-activated microglia conditioned medium (**c**), a combination of Il-1α, TNF and C1q (**d**), LPS-activated microglia conditioned medium pre-treated with neutralizing antibodies to Il-1α, TNF and C1q (**e**), astrocytes treated with Il-1α, TNF and C1q and subsequently treated with FGF (**f**), microglia conditioned medium activated with interferon-γ (IFNγ, **g**), and with TNF (**h**). $n = 6$ per experiment. Data are mean ± s.e.m.

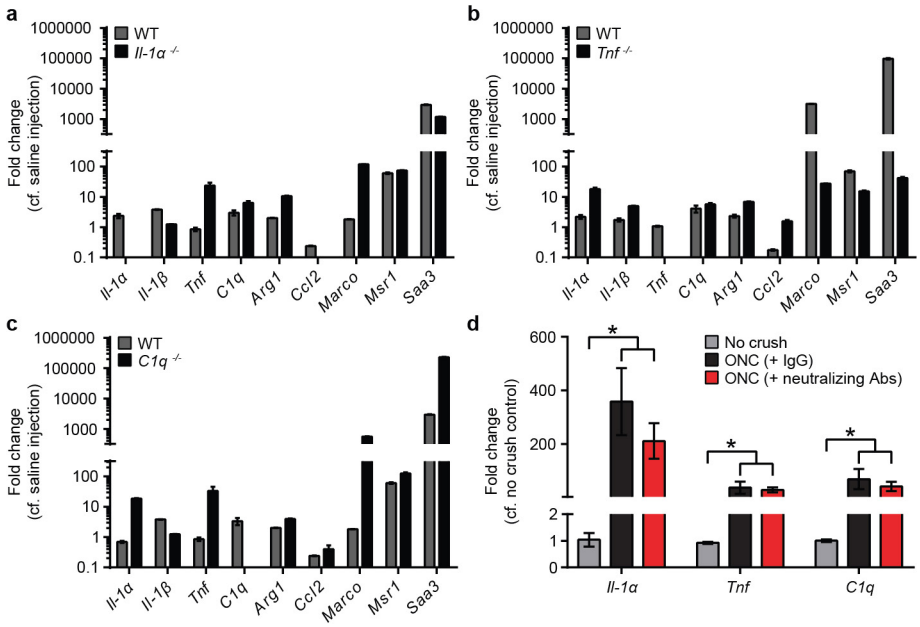

Extended Data Figure 4 | Activation of microglia following systemic LPS injection in knockout mice. a–c, Mice from global single knockouts of Il-1α (**a**), TNF (**b**), and C1q (**c**) were treated with LPS (5 mg/kg, i.p.) and microglia were collected 24 h later. Single-knockout animals still showed upregulation of many markers of microglial activation, as determined by qPCR. $n = 3$ for Il-1α and C1q, $n = 5$ for TNF. **d**, Quantitative PCR for microglia-derived A1-inducing molecules in the optic nerve of mice that received an optic nerve crush. Following crush, the optic nerve contained neuroinflammatory microglia, whereas injection of A1-astrocyte-neutralizing antibodies into the vitreous of the eye did not decrease microglial activation (however it did halt A1 astrocyte activation in the retina, see Fig. 4). Data are mean ± s.e.m. $^*P < 0.05$, one-way ANOVA.

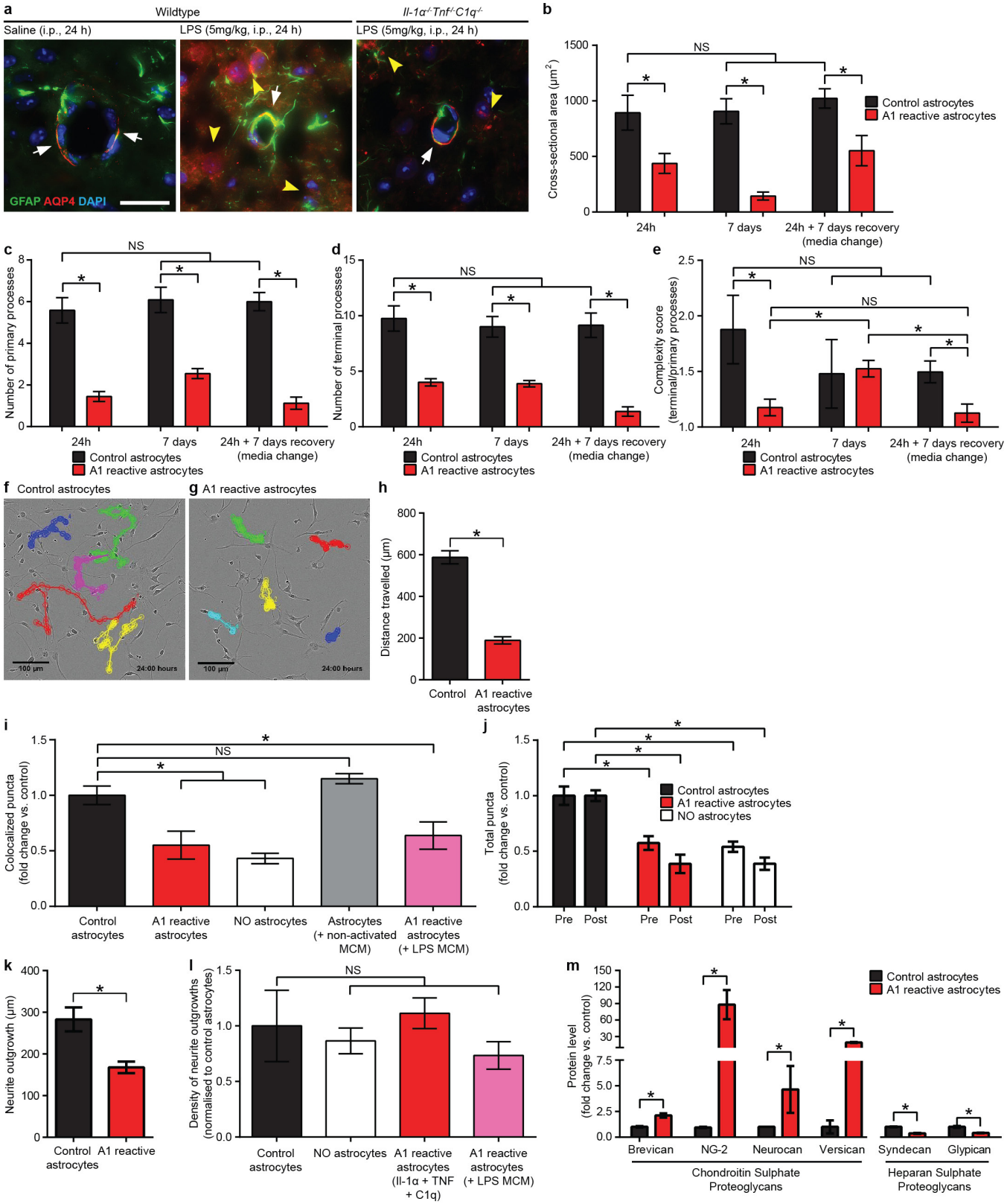

Extended Data Figure 5 | See next page for caption.

Extended Data Figure 5 | A1 astrocytes are morphologically simple and do not promote synapse formation or neurite outgrowth. a, *In vivo* immunofluorescence staining for the water channel AQP4 and GFAP. Saline-injected (control) mice showed robust AQP4 protein localization to astrocytic endfeet on blood vessels (white arrows), whereas LPS-injected mice showed a loss of polarization of AQP4 immunoreactivity, with bleeding of immunoreactivity away from endfeet (white arrows) and increased staining in other regions of the astrocyte (yellow arrowheads). Triple-knockout mice ($Il1a^{-/-}TNF^{-/-}C1qa^{-/-}$) retained AQP4 immunoreactivity in endfeet following LPS-induced neuroinflammation (white arrows), although some low-level ectopic immunoreactivity was still seen (yellow arrowheads). **b**–**e**, Quantification of cell morphology of GFAP-stained cultured astrocytes in resting or A1 reactive state: cross-sectional area (**b**), number of primary processes extending from cell soma (**c**), number of terminal branchlets (**d**), ratio of terminal to primary processes (complexity score, **e**). **f**–**h**, Representative time-lapse tracing of control (**f**) and A1 (**g**) astrocytes. Quantification is shown in **h**. A1 astrocytes migrated approximately 75% less than control astrocytes over a 24-h period. $n = 100$ individual cells from at least 10 separate experiments. **i**, Total number of synapses normalized to each individual RGC. The number of synapses decreased after growth of RGCs with LPS-activated microglial conditioned medium (MCM)-activated A1 astrocyte conditioned medium (ACM), or Il-1α, TNF, C1q-activated (A1 astrocytes) was not different. **j**, Quantification of individual pre- and postsynaptic puncta. **k**, Total length of neurite growth from RGCs. **l**, Density of RGC processes in cultures used for the measurement of synapse number. There was no difference in neurite density close to RGC cell bodies (where synapse number measurements were made). $n = 50$ neurons in each treatment. **m**, Western blot analysis of proteoglycans secreted by control and A1 astrocytes. Conditioned medium from control astrocytes contained less chondroitin sulphate proteoglycans brevican, NG2, neurocan and versican, but contained higher levels of the heparan sulphate proteoglycans syndecan and glypican. $^*P < 0.05$, Student's *t*-test (**d**, **k**) or one-way ANOVA (all other panels). Scale bars, 100 μm. Data are mean $\pm$ s.e.m.

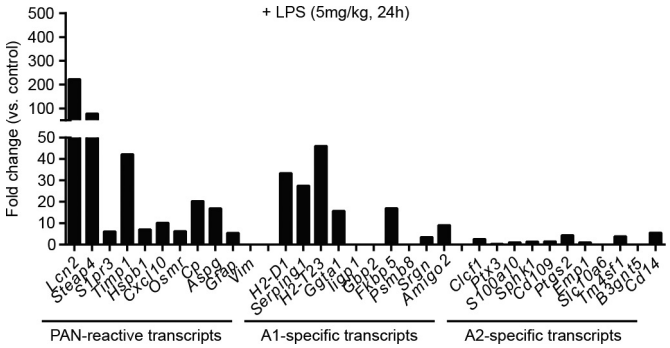

Extended Data Figure 6 | P4 lateral geniculate nucleus astrocytes become A1 astrocytes following systemic LPS injection. Fold change data from microfluidic qPCR analysis of astrocytes purified from dorsal lateral geniculate nucleus of P4 wild-type mice, 24 h after systemic injection with LPS (5 mg kg^{-1}); $n = 2$.

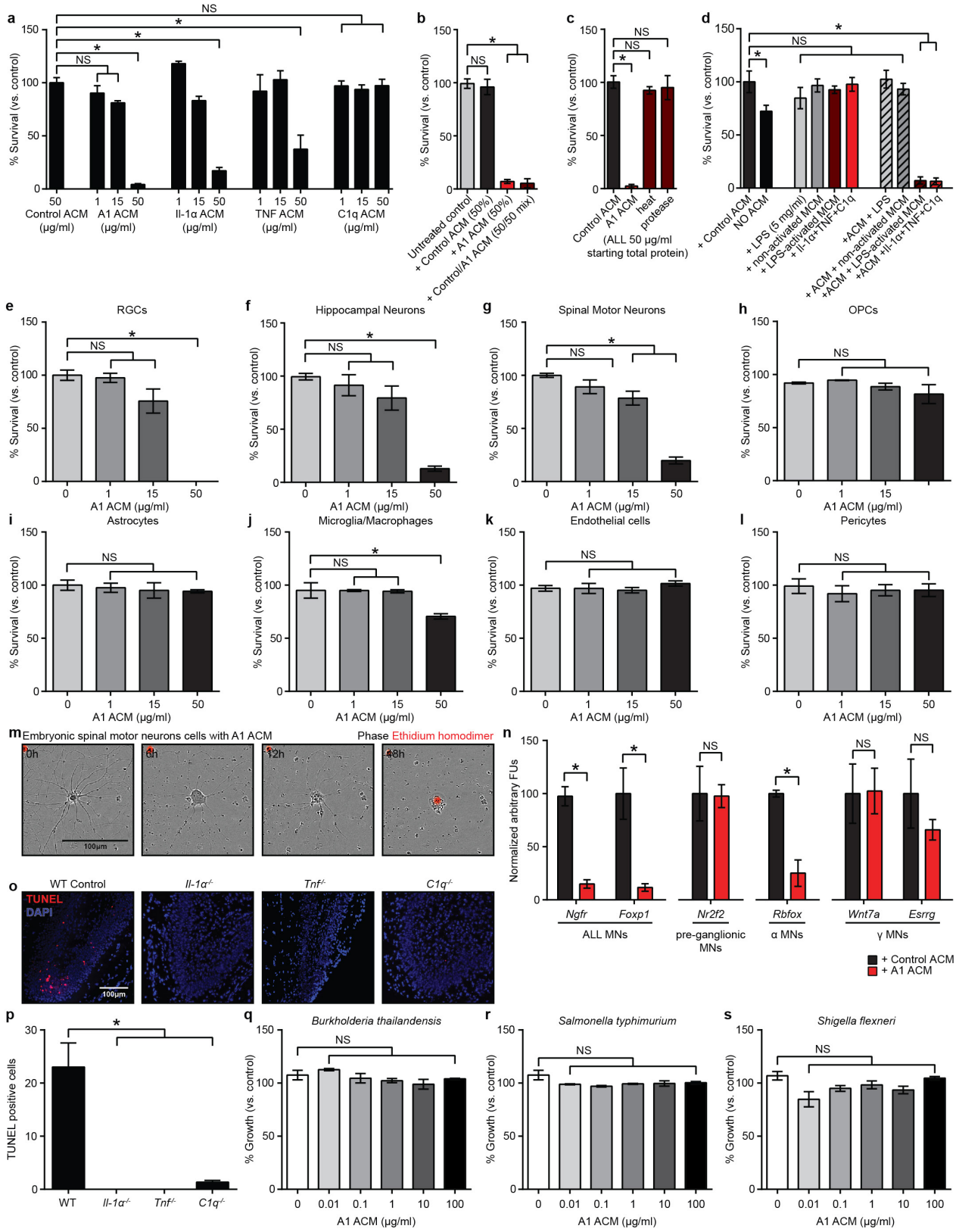

Extended Data Figure 7 | See next page for caption.

Extended Data Figure 7 | A1 astrocytes are strongly neurotoxic. **a**, Quantification of dose-responsive cell death in retinal ganglion cells (RGCs) treated with astrocyte conditioned medium from cells treated with Il-1α, TNF or C1q alone, or combination of all three (A1 astrocyte conditioned medium, ACM) for 24 h. **b**, Death of RGCs was not due to a loss of trophic support, as treatment with 50% control ACM did not decrease viability. Similarly, treatment with a 50/50 mix of control and A1 ACM did not increase viability compared to A1-ACM-only treated cells. **c**, A1-ACM-induced RGC toxicity could be removed by heat inactivation or protease treatment. **d**, LPS treatment alone or microglia conditioned medium (MCM) treatment was unable to kill RGCs. ACM from astrocytes pre-treated with LPS, or non-activated MCM was also unable to kill RGCs. Only ACM from astrocytes treated with LPS-activated MCM or the combination of Il-1α, TNF and C1q (A1 astrocytes) were able to kill RGCs in culture. **e**–**l**, Cell viability of purified CNS cells treated with A1 ACM for 24 h: RGCs (**e**), hippocampal neurons (**f**), embryonic spinal motor neurons (**g**), oligodendrocyte precursor cells (OPCs, **h**), astrocytes (**i**), microglia/macrophages (**j**), endothelial cells (**k**) and pericytes (**l**). $n = 4$ for each experiment. **m**, Representative phase images showing the death of purified embryonic spinal motor neurons in culture over 48 h (ethidium homodimer stain in red shows DNA in dead cells). **n**, qPCR for motor neuronal subtype-specific transcripts after 120 h treatment with A1 ACM (50 μg ml^{-1}). There was no decrease in levels of transcript for *Nr2f2* (pre-ganglionic specific) and *Wnt7a* and *Esrrg* (gamma specific), suggesting these motor neuron subtypes are immune to A1-induced toxicity. $n = 4$ separate primary cultures. **o**, **p**, Representative images (**o**) and quantification (**p**) of terminal deoxynucleotidyl transferase (TdT) dUTP nick-end labelling (TUNEL) staining in the dentate gyrus for wild-type and *Il1a*$^{-/-}$, *TNF*$^{-/-}$ or *C1qa*$^{-/-}$ individual knockout animals following systemic LPS injection. Individual knockout animals had far less TUNEL^{+} cells in the dentate gyrus (no cells in *Il1a*$^{-/-}$ or *TNF*$^{-/-}$ animals) than wild-type animals, suggesting A1-induced toxicity may be apoptosis ($n = 5$). **q**–**s**, Percentage growth rate of gram-negative bacterial cultures treated with A1 ACM for 16 h: *B. thaliandensis* (**q**), *S. typhimurium* (**r**), *S. flexneri* (**s**). $n = 3$; $^{*}P < 0.05$, one-way ANOVA. Data are mean ± s.e.m.

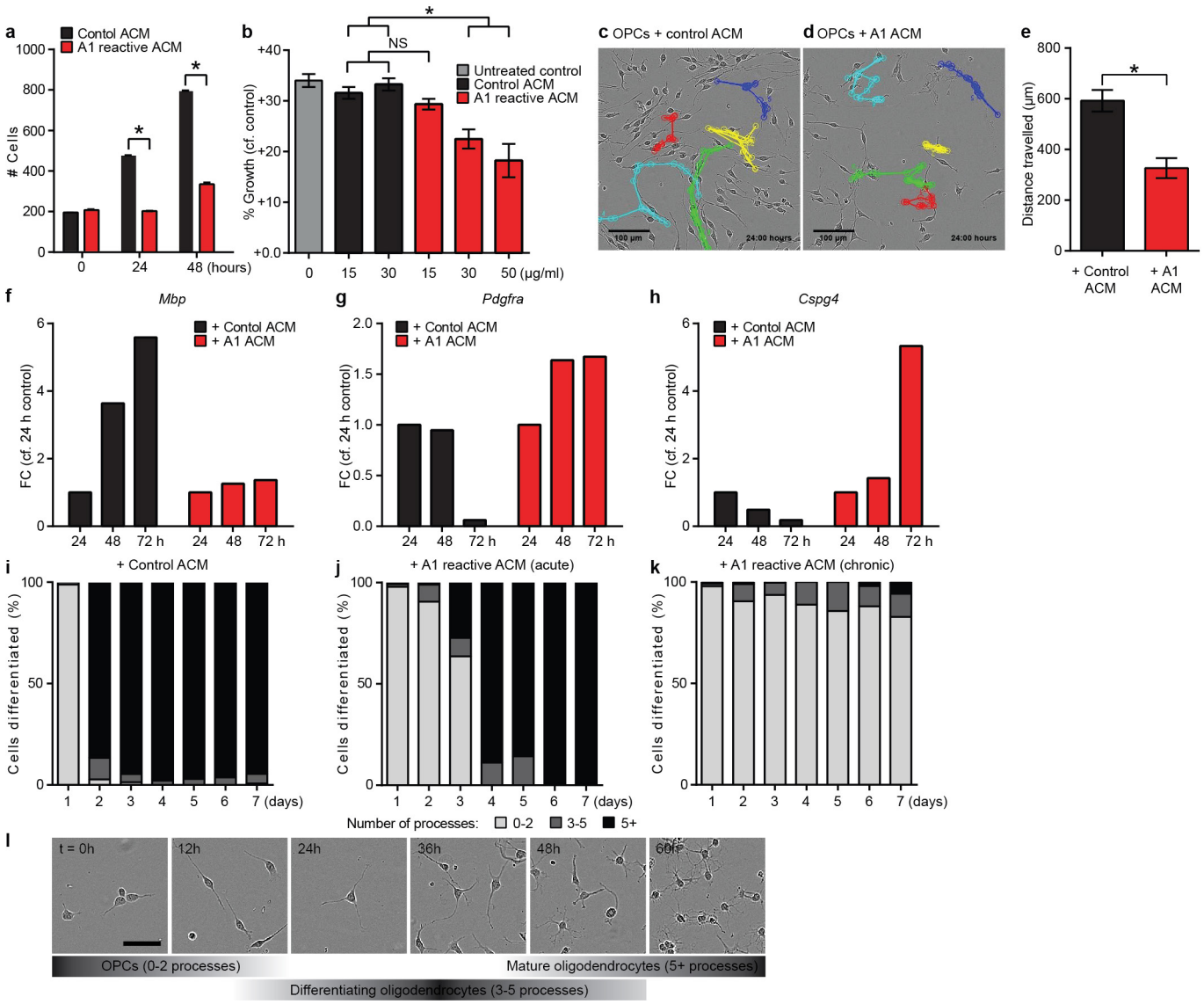

Extended Data Figure 8 | A1 astrocytes inhibit oligodendrocyte precursor cell proliferation, differentiation and migration. a, Number of cells counted from phase-contrast images of oligodendrocyte precursor cells (OPCs) treated with control or A1-conditioned medium (ACM). **b**, EdU-ClickIt-assay-determined growth of OPCs treated with increasing concentrations of control and A1 ACM for 7 days. Both **a** and **b** show that A1 ACM decreases OPC proliferation compared to control. $n = 6$ separate primary cultures each. **c**–**e**, Representative images of time-lapse tracked OPC migration following treatment with control (**c**) and A1 (**d**) ACM, quantified in **e**. $n = 100$ cells from 10 separate experiments. **f**–**h**, qPCR shows no increase in the mature oligodendrocyte marker transcript *Mbp* in rat OPCs treated with A1 ACM, with no change in OPC marker *Pdgfra* and *Cspg4* expression—evidence of a lack of differentiation into mature oligodendrocytes. Treatment of OPCs with control ACM did not delay their differentiation into mature oligodendrocytes ($n = 2$). **i**–**k**, Total number of terminal processes of rat oligodendrocyte lineage cells were counted as a measure of differentiation. Over 90% of cells differentiated by 24 h after removal of PDGFα when treated with control ACM (**i**). By contrast, treatment with a single dose (**j**) or daily doses (**k**) of A1 ACM delayed this level of differentiation up to 72 h following a single dose, or up to the limits of this experiment with chronic treatment. $n = 6$ separate experiments. **l**, Representative phase images and time scale for the oligodendrocyte differentiation assay (treated with control ACM). Scale bars, 100 µm (**c**, **d**) and 25 µm (**l**). $^*P < 0.05$, one-way ANOVA, except for **e** (Student's *t*-test). Data are mean ± s.e.m.

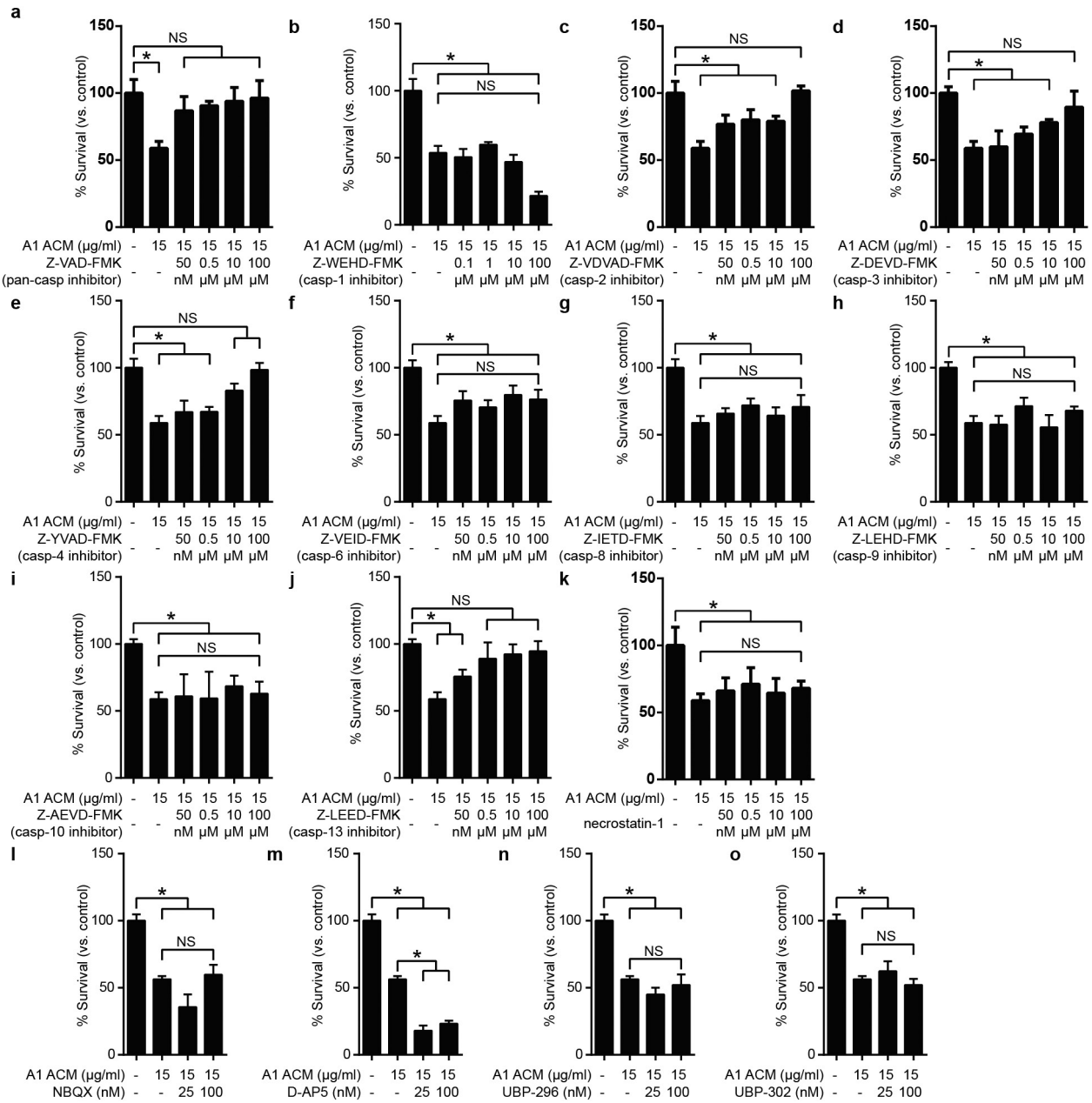

Extended Data Figure 9 | Pharmacological blockade of an astrocyte-derived toxic factor. a–j, Specific caspase inhibitory agents were tested whether these could block retinal ganglion cell (RGC) cell death. **a**, Pan-caspase inhibitor (Z-VAD-FMK). **b**, Caspase-1 inhibitor (Z-WEHD-FMK). **c**, Caspase-2 inhibitor (Z-VDVAD-FMK). **d**, Caspase-3 inhibitor (Z-DEVD-FMK). **e**, Caspase-4 inhibitor (Z-YVAD-FMK). **f**, Caspase-6 inhibitor (Z-VEID-FMK). **g**, Caspase-8 inhibitor (Z-IETD-FMK). **h**, Caspase-9 inhibitor (Z-LEHD-FMK). **i**, Caspase-10 inhibitor (Z-AEVD-FMK). **j**, Caspase-13 inhibitor (Z-LEED-FMK). Only caspase-2, caspase-3, casepase-4 and caspase-13 inhibition was able to minimize RGC toxicity induced by A1 ACM. Cleaved caspase-2 and -3 were detected in dying RGCs (Fig. 4). No cleaved caspase-4 or caspase-13 was detected in these cells. **k**, Necrostatin did not preserve RGC viability when cells were treated with A1 astrocyte conditioned medium (ACM). **l–o**, Glutamate excitotoxicity was checked by blocking AMPA receptors with the antagonist NBQX (**l**), NMDA antagonist D-AP5 (**m**) or kainite receptors with the antagonist UBP-296 (GluR5 selective, **n**) and UBP-302 (**o**)—all of which were ineffective. $^*P < 0.05$, one-way ANOVA, $n = 4$ for each experiment. Data are mean ± s.e.m.

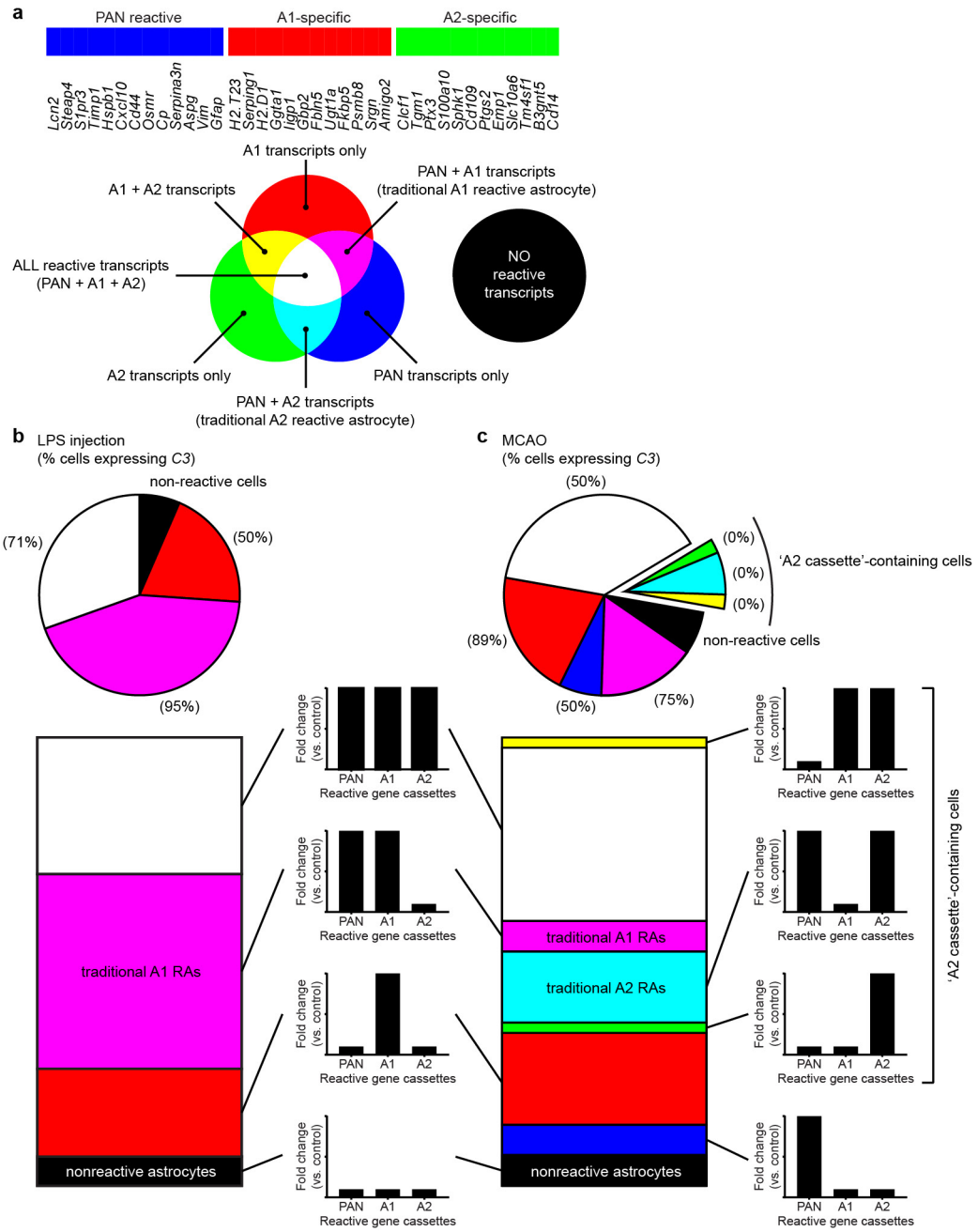

Extended Data Figure 10 | Single-cell analysis of *C3* expression in neuroinflammation and after ischaemic injury. A1 astrocytes were induced with systemic injection of LPS (5 mg kg^{-1}), and A2 astrocytes were induced with middle cerebral artery occlusion in *Aldh1l1–eGFP* mice. Individual astrocytes were collected via FACS and analysed with single-cell microfluidics for astrocyte reactive transcripts. **a**, Cassettes of pan-, A1-, and A2-specific gene transcripts used to determine polarization state of astrocyte reactivity. Upregulation of combinations of each of these cassettes of genes produces eight different possible gene profiles for astrocytes following injury. **b**, 24 h after LPS-induced systemic neuroinflammation, astrocytes were either non-reactive (no reactive genes upregulated), or fell into three forms of reactivity—all with A1 cassette genes upregulated. Numbers in parenthesis show the percentage of individual cells of each subtype expressed *C3*. **c**, 24 h after middle cerebral artery occlusion, both neuroinflammatory (A1 and A1-like) and ischaemic (A2 and A2-like) reactive cells were detected. No cells expressing A2 cassette transcripts were *C3*-positive, validating C3 as an appropriate marker for visualizing A1 astrocytes in disease. Segments of pie charts represent relative amounts of each subtype of astrocyte (control or reactive).

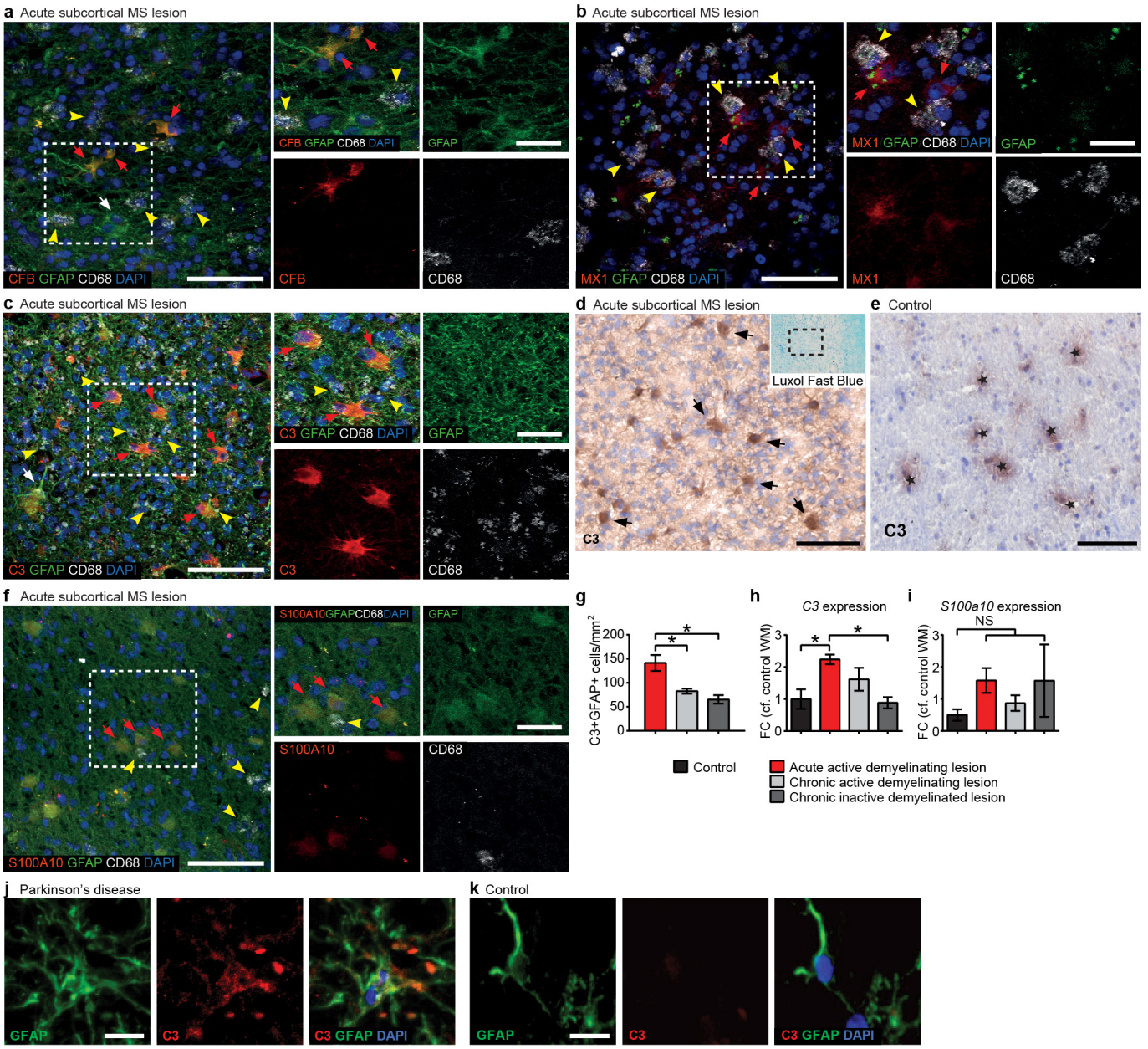

Extended Data Figure 11 | Additional markers for reactive astrocytes in human post-mortem tissue samples. a–h, Multiple Sclerosis (MS). **a–c**, Left, immunofluorescence staining showing CFB (**a**), MX1 (**b**), and C3 (**c**) co-localized with GFAP in cell bodies of reactive astrocytes in acute MS lesions (red arrows). Note the presence of A1-specific GFAP$^+$ reactive astrocytes (C3$^+$, CFB$^+$, MX1$^+$; red arrows) in close proximity to CD68$^+$ phagocytes (activated microglia, macrophages; yellow arrowheads); A1-specific astrocytes are predominantly seen in high CD68$^+$ density areas. C3$^-$GFAP$^+$ astrocytes (white arrows). Right, single channel and higher magnification images of selected areas of **a–c**. **d**, Immunohistochemical staining for C3 shows that it is strongly upregulated in astrocytes in active MS lesions. These astrocytes have a hypertrophic morphology with retracted processes (black arrows). Note hypercellularity indicating extensive infiltration by inflammatory cells in an active demyelinating MS lesion of subcortical white matter (compared to the luxol fast blue myelin stain of the lesion area in the right upper corner). **e**, C3 staining pattern in subcortical control white matter is mainly associated with blood vessels (stars). **f**, The A2-specific marker S100A10 did not co-localize with C3$^+$ A1 astrocytes, although some S100A10$^+$ cells were present in acute subcortical MS lesions. **g**, The number of C3$^+$GFAP$^+$ co-labelled cells was highest in acute active demyelinating lesions, however they were still present in chronic active and inactive lesions. **h**, There was a matching increase in *C3* transcript in brains of patients with acute active demyelinating lesions compared to age-matched controls. FC, fold change. **i**, There was no difference in the expression of *S100a10* in these same patient samples. $n = 3$–8 disease and 5–8 control for each experiment. Quantification was carried out on 5 fields of view and approximately 50 cells were surveyed per sample. **j**, **k**, Substantia nigra from patients with Parkinson's disease (**j**) and age-matched controls (**k**). Additional representative images of C3$^+$GFAP$^+$ co-labelled cells in the substantia nigra of patients with Parkinson's disease (**j**). No C3$^+$ reactive astrocytes were seen in age-matched control substantia nigra (**k**). Scale bars, 100 μm (**a–f**), 20 μm (**j**, **k** and enlarged inserts). Data are mean ± s.e.m. $^*P < 0.05$, one-way ANOVA, compared to age-matched control.